

## TITLE PAGE

### **Oxygen enhanced-MRI is feasible, repeatable and detects radiotherapy-induced change in hypoxia in xenograft models and in patients with non-small cell lung cancer**

Ahmed Salem<sup>1, 2, 3</sup>, Ross A Little<sup>2</sup>, Ayşe Latif<sup>4</sup>, Adam K Featherstone<sup>2</sup>, Muhammad Babur<sup>4</sup>, Isabel Peset<sup>5</sup>, Susan Cheung<sup>2</sup>, Yvonne Watson<sup>2</sup>, Victoria Tessyman<sup>4</sup>, Hitesh Mistry<sup>4</sup>, Garry Ashton<sup>6</sup>, Caron Behan<sup>6</sup>, Julian C Matthews<sup>7</sup>, Marie-Claude Asselin<sup>2</sup>, Robert G Bristow<sup>1, 3</sup>, Alan Jackson<sup>2</sup>, Geoff JM Parker<sup>2, 8</sup>, Corinne Faivre-Finn<sup>1, 3</sup>, Kaye J Williams<sup>4</sup> \* and James PB O'Connor<sup>1, 9</sup> \*

<sup>1</sup>: Division of Cancer Sciences, University of Manchester, Manchester, UK.

<sup>2</sup>: Division of Informatics Imaging & Data Sciences, University of Manchester, Manchester, UK.

<sup>3</sup>: Department of Clinical Oncology, The Christie Hospital NHS Trust, Manchester, UK.

<sup>4</sup>: Division of Pharmacy, University of Manchester, Manchester, UK

<sup>5</sup>: Imaging and Flow Cytometry, Cancer Research UK Manchester Institute, Manchester, UK

<sup>6</sup>: Histology, Cancer Research UK Manchester Institute, Manchester, UK

<sup>7</sup>: Division of Neuroscience and Experimental Psychology, University of Manchester, Manchester, UK

<sup>8</sup>: Bioxydyn Limited, Manchester, UK.

<sup>9</sup>: Department of Radiology, The Christie Hospital NHS Trust, Manchester, UK.

\* These authors contributed equally

**Running title:** OE-MRI detects radiotherapy-induced hypoxia modification

**Key words:** Biomarker; Hypoxia; Magnetic Resonance Imaging; Personalized medicine; Radiotherapy

**Financial support:** This study was funded by the Engineering and Physical Sciences Research Council and Cancer Research UK (CRUK) (grant C8742/A18097; 2013-2018). This study was supported by researchers at the NIHR Manchester Biomedical Research Centre. AS was supported by an Early Careers Fellowship from Manchester Cancer Research Centre and The Christie Charity and

by a University of Manchester Presidential Fellowship for Clinicians. JPBO'C is supported by Cancer Research UK (C19221/A15267, C19221/A22746). Clinical OE-MRI was supported by Philips through a research agreement with The University of Manchester.

**Corresponding author:**

James O'Connor MA PhD FRCR  
Division of Cancer Sciences  
University of Manchester  
Manchester  
M20 4BX, UK  
Tel. + 44 161 446 3896  
E-mail: James.O'Connor@manchester.ac.uk

**Conflict of interest disclosure statement:** GJMP has no competing interests directly relating to this manuscript. Activities not related to the present article: disclosed board membership at Bioxydyn; consultancy at GlaxoSmithKline; employment at Bioxydyn; receives royalties from the University of Manchester for patents on commercial software; owns stock and stock options in Bioxydyn; money to author for three patents relating to oxygen-enhanced MRI from Bioxydyn. None of the other authors have any competing financial or non-financial interests.

**Author contributions:**

AS and JPBO'C are guarantors of integrity of the entire study; AS, AJ, CFF, GJMP, KJW and JPBO'C came up with the study concept and designed the study; AS, MB, IP, YW, AL and JPBO'C acquired the study data; AS, RAL, AKF, IP, SC, YW, AL, VT, HM, CB and JPBO'C analyzed the study data; HM provided statistical input; all authors contributed to the interpretation of the data, manuscript drafting and revision for important intellectual content and approved the final version of the submitted manuscript.

**Word count:** 4,946 words

**Number of figures:** 5

**Number of tables:** 1

## STATEMENT OF TRANSLATIONAL RELEVANCE

Hypoxia is a negative prognostic indicator and predicts poor outcome for cancer treatments including radiotherapy, chemotherapy, and immunotherapy. Currently no validated tests are routinely available to detect and track tumor hypoxia to guide clinical decision-making. Here, we report the first evidence to support using oxygen-enhanced MRI (OE-MRI) for this role. Preclinical experiments in two xenograft models demonstrated that the combined OE-MRI and dynamic contrast-enhanced MRI (DCE-MRI) biomarker *perfused Oxy-R volume* can identify, map, and quantify (chemo)radiotherapy-induced tumor hypoxia change. We then translated this imaging method into the clinic demonstrating feasibility and that *perfused Oxy-R volume* is repeatable and can detect chemoradiotherapy-induced hypoxia changes in patients with NSCLC. Our data support applying OE-MRI to monitor hypoxia-modification, to stratify patients in hypoxia-targeted drug trials, to identify patients with hypoxic tumors that may fail anticancer treatment such as immunotherapy, and to guide adaptive radiotherapy dose painting by mapping regional hypoxia.

## ABSTRACT

**Background:** Hypoxia is associated with poor prognosis and is predictive of poor response to cancer treatments, including radiotherapy. Developing non-invasive biomarkers that both detect hypoxia prior to treatment and track change in tumor hypoxia following treatment is required urgently.

**Experimental Design:** We evaluated the ability of oxygen-enhanced MRI (OE-MRI) to map and quantify therapy-induced changes in tumor hypoxia by measuring *oxygen-refractory* signals in perfused tissue (*perfused Oxy-R*). Clinical first-in-human study in patients with non-small cell lung cancer (NSCLC) was performed alongside preclinical experiments in two xenograft tumors (Calu6 NSCLC model and U87 glioma model).

**Results:** MRI *perfused Oxy-R* tumor fraction measurement of hypoxia was validated with *ex vivo* tissue pathology in both xenograft models. Calu6 and U87 experiments showed that MRI *perfused Oxy-R* tumor volume was reduced relative to control following single fraction 10 Gy radiation and fractionated chemoradiotherapy ( $p < 0.001$ ) due to both improved perfusion and reduced oxygen consumption rate. Next, evaluation of 23 NSCLC patients showed that OE-MRI was clinically feasible and that tumor *perfused Oxy-R* volume is repeatable (interclass correlation coefficient: 0.961 (95% CI 0.858-0.990); coefficient of variation: 25.880%). Group-wise *perfused Oxy-R* volume was reduced at 14 days following start of radiotherapy ( $p = 0.015$ ). OE-MRI detected between-subject variation in hypoxia modification in both xenograft and patient tumors.

**Conclusions:** These findings support applying OE-MRI to monitor hypoxia-modification, to stratify patients in clinical trials of hypoxia-modifying therapies, to identify patients with hypoxic tumors that may fail treatment with immunotherapy, and to guide adaptive radiotherapy by mapping regional hypoxia.

## INTRODUCTION

Most solid tumors contain sub-regions of hypoxia. The presence and degree of hypoxia has long been recognized as an important negative prognostic factor in cancer (1,2). Furthermore, hypoxia predicts poor outcome following surgery (3), radiotherapy (4) and chemotherapy (5), and is associated with relapse and progression (6). Therefore, patients with highly hypoxic tumors tend to have decreased overall cancer survival following conventional therapies (7). Recently, there is evidence that targeted therapies such as immunotherapy may be less effective in hypoxic tumors (8,9). For these reasons, there is an unmet need to target hypoxia to improve cancer outcomes (10).

Positron emission tomography (PET) methods have shown that imaging can provide serial non-invasive *in vivo* measurement of tumor hypoxia, can track hypoxia modification, and has potential to stratify patients and personalize their therapy (11-13). However, hypoxia PET approaches are limited currently to specialist centres, hindering widespread use in clinical trials and adoption into clinical practice (14). Proton MRI is used widely in the clinic, making it an attractive alternative to PET for measuring oxygen delivery and hypoxia in tumors. Oxygen-enhanced MRI (OE-MRI) measures the change in longitudinal relaxation rate of tissue protons ( $R_1$ ) (15). Preclinical studies have shown that the OE-MRI biomarker '*perfused Oxy-R*' distinguishes hypoxic tumor regions from well-oxygenated regions, where analysis is performed in perfused tumor sub-regions (identified by dynamic contrast-enhanced MRI (DCE-MRI)) (16).

We hypothesized that *perfused Oxy-R* could spatially map and quantify changes in tumor hypoxia induced by radiotherapy (RT) and chemoradiotherapy (CRT). To test this, we evaluated changes in *perfused Oxy-R* induced following RT or CRT in two xenograft models. We validated our findings with *ex vivo* immunohistochemistry and oxygen consumption rate (OCR) assays. We then performed a first-in-human study in patients with non-small cell lung cancer (NSCLC) to demonstrate feasibility and repeatability and to see if equivalent findings were observed. Finally, we investigated if *perfused Oxy-R* could detect inter-subject heterogeneity in hypoxia-modification between patients to support a potential role for OE-MRI in personalized medicine.

## MATERIALS AND METHODS

### ***Preclinical study design***

Studies complied with UK guidelines on animal welfare in cancer research (17) and received approval from the Animal Welfare and Ethical Review Body. Preclinical experiments were performed in Calu-6 NSCLC xenografts and in U87 glioma xenografts.

Tumors were propagated by injecting either 0.1 ml of Calu-6 NSCLC cells ( $2 \times 10^7$  cells/ml) or 0.1 ml of U87 cells ( $5 \times 10^6$  cells/ml) intra-dermally in the lower back of CD1 nude mice. When tumors reached  $>200 \text{ mm}^3$  by caliper measurement, mice were entered into the study (assigned as day 0). They were imaged while anaesthetized using 2% isoflurane carried initially in medical air (21% oxygen), before switching the 100% oxygen as part of the OE-MRI protocol. Core temperature was controlled at 36°C.

After initial imaging (day 0), mice were randomized to pathology validation only, control/sham or given treatment with tumor-localized RT. This was administered using a metal-ceramic MXR-320/36 X-ray machine (320kV, Comet AG, Switzerland) under ambient conditions to restrained, non-anaesthetized mice held in a lead-shielded support perpendicular to the source. Irradiation was delivered at a dose rate of 0.75 Gy/min. Mice were turned around halfway through the procedure to ensure uniform tumor dose.

### ***Preclinical MRI data acquisition and analysis***

For Calu-6 xenograft MRI experiments (**supplementary figure 1A**), groups were:

- a) MRI-pathology validation (N=7) with single MRI scan, followed by tumor harvest;
- b) Treatment effect: control group (N=9); treatment with single 10 Gy fraction of RT (N=9); treatment with fractionated 5 x daily 2 Gy RT with concurrent cisplatin on day 0; CRT (N=6). Initial MRI was at day 0 after which therapy was administered. Subsequent MRI was performed at days 3, 6, and 10 in all groups and then at day 14 (control), day 18 and 24 (RT), and day 18 (CRT).

For U87 xenograft MRI experiments (**supplementary figure 1B**), groups were:

- a) MRI-pathology validation (N=10) with single MRI scan, followed by tumor harvest;

- b) Treatment effect: control group (N=10); treatment with single 10 Gy fraction of RT (N=13). Initial MRI was at day 0 after which therapy was administered. Subsequent MRI was performed at day 3 only (control) or at days 3, 6, 10 and 24 (RT).

Imaging was performed using a volume transceiver coil on a 7 T Magnex instrument interfaced to a Bruker Avance III console and gradient system. After initial localizer and  $T_2$ -weighted anatomy scans, mice underwent coronal imaging. OE-MRI consisted of a variable flip angle (VFA) spoiled gradient echo (SPGR) acquisition to calculate native tissue  $R_1$  ( $1/T_1$ ; unit  $s^{-1}$ ; TR = 30 ms; TE = 1.44 ms;  $\alpha = 5^\circ/10^\circ/20^\circ$ ). This was followed by 42 dynamic  $T_1$ -weighted spoiled gradient recalled acquisitions in the steady state (SPGR; TR = 30 ms; TE = 1.44 ms;  $\alpha = 20^\circ$ ; temporal resolution: 28.8 s). After 18 acquisitions, gas delivered through a nose cone was switched to 100% oxygen. Details of preclinical DCE-MRI acquisition are described in **supplementary methods**.

Regions of interest (ROI) were defined by a research radiographer (YW, 18 years' experience) using Jim 7 (Xinapse Systems, West Bergholt, Essex, UK). For OE-MRI, voxel-wise  $\Delta R_1$  were calculated for each voxel, where  $\Delta R_1 = R_1$  while breathing oxygen (last 18 of 24 time points on 100% oxygen) minus  $R_1$  on breathing air (18 time points on medical air). Tumor average  $\Delta R_1$  was calculated as the median value. Voxels were classified as oxygen-enhancing (*Oxy-E*) if the  $\Delta R_1$  was positive and significant (one sided paired sample  $t$ -test between pre-oxygen and oxygen-breathing time points,  $p < 0.05$ ). All other voxels were defined as refractory to oxygen challenge (*Oxy-R*).

DCE-MRI was then used to classify tumor voxels as non-perfused (where initial area under the Gd contrast agent concentration-time curve at 60 s ( $IAUC_{60}$ ; units  $mmol/l$ ;  $\leq 0$ )) or perfused (where  $IAUC_{60} > 0$ ). Together, these co-registered voxel-wise OE-MRI and DCE-MRI data were combined to distinguish *perfused Oxy-E* (normoxia), *perfused Oxy-R* (hypoxia) and non-perfused (necrosis) voxels, based on previously published methods (18) (**supplementary figure 2A**).

### ***Xenograft pathology analysis***

For Calu-6 xenografts, three datasets were used. The first pathology experiment compared the hypoxic fractions measured on an immunohistochemistry image from the centre of each tumor with a single MRI slice acquired in the same plane from the

corresponding tumor region, to validate OE-MRI measurements of hypoxia (**supplementary figure 1A**). The next two pathology experiments evaluated change in hypoxia following therapy. We evaluated tumor size-matched data obtained at tumor harvest from the mice that underwent the MRI study (details above; **supplementary figure 1A**) and separate *time*-matched data acquired in non-imaged mice at day 10, guided by the MRI experiment. This additional experiment had control (N=9), and tumors treated with single 10 Gy fraction of radiotherapy (N=6) (**supplementary figure 1C**). For U87 xenografts, size-matched data were obtained at tumor harvest from the mice that underwent MRI (details above; **supplementary figure 1B**). Pimonidazole data acquisition and analysis details are described in **supplementary methods**.

### ***Xenograft oxygen consumption rate analysis***

A fourth Calu-6 xenograft cohort was used separate to those used for MRI and pathology analysis. Tissue biopsy preparation protocols were adapted from a published method (19) and are described in **supplementary methods**. Separate mouse cohorts were used: Calu-6 xenograft groups were *time*-matched control (N=7), size-matched control (N=5), and treated with single 10 Gy fraction of RT (N=6) (**supplementary figure 1D**). Five consecutive basal OCR measurements were performed for all samples.

Since previous work (19) has shown that percentage viability and necrotic fraction of tumors is directly proportional to observed oxygen consumption, we used H&E staining to quantify necrotic fraction for each sample using a scoring method based on level of nuclear staining. Following OCR measurements, the samples were imaged using Oxford Optronix GelCount™ (Oxford Optronix Ltd., Abingdon, UK). Necrotic areas were calculated using ImageJ software. Whole field H&E images, representative biopsy sections and the scoring method devised to quantify necrosis are shown in **supplementary figure 3**.

### ***Clinical study design, patient population and treatment***

NSCLC patients eligible for curative-intent RT alone or combined CRT (either concurrent or sequential) were recruited prospectively from The Christie NHS Foundation Trust (Manchester, UK) following local research and development and institutional review board approval (reference: 15/NW/0264, CPMS ID: 18870). This study was conducted in accordance with the Declaration of Helsinki

All patients were  $\geq 18$  years old, had histologically- or cytologically-confirmed NSCLC, and provided written informed consent. Eligible participants also had ECOG performance score of  $\leq 2$ , serum creatinine  $< 120$   $\mu\text{mol/L}$  or calculated creatinine clearance (Cockcroft–Gault)  $\geq 30$  mL/min. Patients with distant metastasis were included only if eligible for curative-intent therapy. Patients with contraindications to MRI were excluded. Coexistent chronic obstructive pulmonary disease was allowed, but patients were required to have adequate lung function as part of standard radiotherapy workup (forced expiratory volume in 1 second greater than 1 liter, or  $> 40\%$  predicted value).

We examined safety (defined as no adverse events reported or detected on clinical examination) and tolerability (defined as completion of the imaging protocol) in a development cohort (N=6 patients). Based on these data, the study recruited an expansion cohort to evaluate MRI biomarker repeatability and sensitivity to treatment effect (N=17 patients). The study design is summarized in **supplementary figure 4**.

RT planning was performed using 3-dimensional or 4-dimensional CT. Treatment was delivered with intensity-modulated radiotherapy on a linear accelerator (55 Gy in 20 daily fractions or 60-66 Gy in 30-33 daily fractions). Patients receiving concurrent CRT had cisplatin and etoposide administered. Patients receiving sequential CRT had cisplatin or carboplatin administered with either gemcitabine (if squamous cell carcinoma) or pemetrexed (if adenocarcinoma). In sequential CRT treated patients, repeat imaging was performed after completion of chemotherapy. Toxicity was assessed by a clinical oncologist (AS; 8 years' experience) prior to and after each scan. No pre-defined standardized follow-up diagnostic scans were mandated after completion of the research imaging protocol

### ***Clinical MRI data acquisition and analysis***

All MRI data were acquired free breathing on a 1.5 T whole body scanner (Philips Achieva, Philips Medical Systems, Best, Netherlands) using the Q Body (OE-MRI) and Sense XL Torso (DCE-MRI) coils. After initial localizer and anatomical scans, patients underwent OE-MRI and DCE-MRI. Scan duration was approximately 45 min (summarized in **supplementary figure 5A**). All sequences were co-localized and acquired in the coronal plane with FOV 450 mm x 450 mm x 205 mm; and 5 mm thick slices. Anatomical scans in-plane resolution was 1.76 mm x 1.76 mm, whereas OE-MRI and DCE-MRI images had in-plane resolution of 4.69 mm x 4.69 mm.

For OE-MRI,  $R_1$  was calculated using a series of coronal 3D single shot inversion recovery prepared SPGR acquisitions (TR = 2.1 ms; TE = 0.50 ms;  $\alpha = 6^\circ$ , number of excitations = 5, TI: 10, 50, 300, 1100, 2000, 5000 ms). Dynamic images were acquired at TI of 1100 ms. For the first 6 patients in the protocol development cohort, 12 measurements were acquired while breathing medical air (21% oxygen) to determine native  $R_1$  prior to oxygen challenge. This was increased to 18 for all subsequent patients following an interim study review. Measurements on air were followed, in all patients, by 48 measurements after gas switch to 100% oxygen (flow rate: 15 l/min) and a final 30 following switch back to medical air (temporal resolution: 10 s). Gases were delivered using a tight-sealed, non-rebreathing Intersurgical EcoLite™ Hudson facemask (Intersurgical Ltd, Berkshire, UK) via a gas blender, allowing switching between gases. A two-step quality assurance procedure was applied to ensure successful delivery of the gas challenge. First, 100% oxygen challenge delivery was confirmed in all scans at the time of image acquisition via a gas-sensing probe placed inside the facemask and connected to a gas analyzer (ADInstruments Pty Ltd, Bella Vista, Australia; **supplementary figure 5B**). Second,  $R_1$  was measured in the descending thoracic aorta, outlined by a clinical oncologist (AS), to provide a positive control by detecting indirect oxygen input function to the tumor. Details of clinical DCE-MRI acquisition are described in **supplementary methods**. Representative pre-processed OE-MRI and DCE-MRI acquisitions are shown in **supplementary video 1A**.

Tumor ROIs were defined by a clinical oncologist (AS) and reviewed by a board certified clinical radiologist (JPBOC; 14 years' experience), using Jim 7 on coronal pre- and post-Gd  $T_1$ -weighted images, guided by diagnostic [ $^{18}\text{F}$ ]fluorodeoxyglucose (FDG) PET CT images.

For OE-MRI, whole tumor and voxel-wise  $\Delta R_1$  were calculated, where  $\Delta R_1 = R_1$  while breathing oxygen (mean of last 18 time points on 100% oxygen) minus  $R_1$  on breathing air (mean of acquisitions on medical air). Voxels were classified as *Oxy-E* if the  $\Delta R_1$  was positive and significant (one sided paired sample  $t$ -test between pre-oxygen and oxygen-breathing time points,  $p < 0.05$ ). All other voxels were defined as *Oxy-R*.

For DCE-MRI, tumor median  $IAUC_{60}$  was also calculated. Voxels were classified as perfused when the area under the Gd contrast agent concentration curve was  $> 0$  (one sided paired sample  $t$ -test,  $p < 0.005$ ) (20). Voxel-wise OE-MRI and DCE-MRI

data were combined to distinguish *perfused Oxy-E* (normoxia), *perfused Oxy-R* (hypoxia) and non-perfused voxels (necrosis), based on previously published methods and with an identical approach to that used in the preclinical experiments (18) (**supplementary figure 2B**), using data corrected for breathing and bulk patient motion (details in **supplementary methods and supplementary video 1B**).

### **Statistical analysis**

All statistical analyses were performed in IBM SPSS Statistics version 22.0 (IBM Corp., Armonk, NY, USA). For all preclinical data, tumor growth rate comparisons were assessed using a log rank test for time to double tumor volume. Pearson's correlation analysis was used to assess relationships between pre-treatment MRI parameters and immunohistochemistry. Two-sample unpaired *t*-tests were performed to assess differences in mean sub-region fractions and volumes (*perfused Oxy-R*, *perfused Oxy-E* and non-perfused), immunohistochemistry or OCR assay between control and treated groups at specific time-points of interest. Corresponding *p*-values are reported and were considered statistically significant when  $p < 0.05$  (two-sided). No corrections for multiple comparisons were made.

For both preclinical and clinical MRI, changes in *perfused Oxy-R* volume of  $>50\%$  were considered significant. This threshold was based on similar studies of other functional imaging biomarkers, where parameter changes of 40-50% are considered significant (21). For clinical data descriptive statistics were presented using median and 95% confidence intervals (CI) or standard deviation.

For the clinical study, pre-study sample size calculations were not performed as this was a first-in-human proof-of-concept study. Single measures two-way mixed effects model absolute agreement interclass correlation coefficient (ICC) and coefficient of variation (CoV) were calculated for summary OE-MRI parameters and the hypoxia biomarker *perfused Oxy-R* between repeat acquisitions (together with their respective 95% CI). Recommendations (22) that interpret ICC values between 0.75-0.9 and greater than 0.9 as indicative of good and excellent repeatability, respectively, were used. In addition, Bland-Altman analysis was performed to calculate bias and 95% limits of agreement ( $LoA = 1.96 \times \text{standard deviation}$ ).

## **RESULTS**

### ***Perfused Oxy-R identifies and quantifies hypoxic volumes in xenograft models***

Calu-6 xenografts (23,24) and U87 xenografts (25) were chosen for the study since these models contain moderate to high levels of hypoxia. We measured the MRI *perfused Oxy-R* fraction (**supplementary figure 2A**) on one central slice of the tumor to provide *in vivo* quantification of hypoxia. *Perfused Oxy-R* fraction correlated significantly with the hypoxic fraction measured by pimonidazole immunohistochemistry, for both Calu-6 xenografts ( $R^2=0.700$ ;  $p=0.019$ ) (**figure 1A**) and U87 xenografts ( $R^2=0.447$ ;  $p=0.035$ ) (**figure 1B**). No relationship was detected between pimonidazole immunohistochemistry measurement of hypoxia and  $IAUC_{60}$ . (**supplementary figure 6A-B**) These data provide pathological validation that an OE-MRI biomarker measured in perfused tumor, but not DCE-MRI derived  $IAUC_{60}$ , quantifies tumor hypoxia in Calu-6 and U87 xenografts.

Data were obtained across a size range that was representative of all subsequent experiments (tumor sizes: 191 to 974 mm<sup>3</sup> measured by MRI volumetrics). No significant relationship was seen between pimonidazole immunohistochemistry measurement of hypoxia and tumor size (representative images in **figure 1C-D**; **supplementary figure 6C-D**). This highlights that tumor size and hypoxia are independent of one another in both xenograft models used in this study.

### ***Perfused Oxy-R detects radiotherapy-induced hypoxia modification in xenograft models***

Calu-6 xenografts treated with either RT (single fraction of 10 Gy) or CRT (5 x 2 Gy fractions plus cisplatin) exhibited significant growth delay relative to control xenografts ( $p<0.001$ ), assessed by measuring time to double in tumor volume.

To understand the dependence of 3-dimensional growth inhibition on tumor hypoxia, we measured change in *perfused Oxy-R* volume within each tumor. Since growth inhibition was clearly apparent by day 10 (**figure 2A**), we assessed OE-MRI at this time point. By day 10, *perfused Oxy-R* volume was reduced in xenografts treated with RT ( $p=0.029$ ) or fractionated CRT ( $p=0.047$ ), relative to control (**figure 2B**). Hypoxia modification persisted until tumor harvest (CRT group at day 18; RT group at day 24; both  $p<0.001$ ). OE-MRI maps showed spatially coherent changes in hypoxia (**figure 2C**). In distinction, median change in  $\Delta R_1$  – a commonly reported biomarker in OE-MRI (26) – showed borderline significance only at day 6 and 10 (**supplementary figure 7**).

We analyzed pimonidazole immunohistochemistry performed at day 10 in a separate cohort of Calu-6 xenografts. Lower hypoxic fraction was seen in tumors treated with RT ( $p=0.026$ ), relative to *time*-matched controls (**figure 2D**). Next, we performed pimonidazole immunohistochemistry analysis of the xenografts undergoing MRI. Lower hypoxic fractions in RT ( $p=0.042$ ) and CRT ( $p=0.041$ ) were found in treated tumors, relative to *size*-matched control (**figure 2E-F; supplementary figure 8**).

Experiments were repeated in U87 tumors. Xenografts treated with single fraction of 10 Gy RT exhibited significant growth delay, relative to control xenografts ( $p<0.001$ ) (**supplementary figure 9A**). *Perfused Oxy-R* volume was decreased in RT treated ( $p=0.07$ ), relative to control by day 3 and this reduction persisted until day 10 (**supplementary figure 9B**). Sample OE-MRI maps are shown (**supplementary figure 9C**). Pimonidazole immunohistochemistry confirmed that lower hypoxic fractions were observed in RT treated tumors ( $p=0.002$ ), relative to *size*-matched control (**supplementary figure 9D**). Collectively these data provide pathological validation that this OE-MRI biomarker detects hypoxia-modification induced by radiotherapy in two xenograft models.

#### ***Hypoxia modification detected by perfused Oxy-R is due to alterations in blood flow and oxygen consumption***

To investigate the mechanistic basis for the reduction in hypoxia following treatment we examined dynamic change in tumor vascular status measured on DCE-MRI from day 0 to tumor harvest and also single measurement of OCR at day 10. DCE-MRI data showed that  $IAUC_{60}$  was increased significantly at days 6-10 in Calu-6 xenografts in both the RT and CRT treated groups, relative to control ( $p<0.001$ ). These changes also persisted to day 24 in the group treated with single 10 Gy RT (**figure 3A-B**). Equivalent data were observed in U87 xenografts (**supplementary figure 10**).

Fresh biopsy samples were taken from Calu-6 xenografts in three groups: control *time*-matched tumors (average volume  $637\pm 52\text{mm}^3$ ) at day 10 post sham treatment; control *size*-matched tumors (average volume  $242\pm 27\text{mm}^3$ ); and RT treated tumors at day 10 post single 10 Gy fraction (average volume  $271\pm 15\text{mm}^3$ ). The mean of the five consecutive basal OCR measurements performed over 30 minutes under ambient conditions was significantly reduced by RT compared with *time*- ( $p=0.008$ ) and *size*-matched ( $p<0.001$ ) controls (**figure 3C**). Necrotic scoring revealed no

significant differences between the irradiated and *time-* or *size-*matched controls (**figure 3D**), indicating equivalent levels of tissue viability between the three groups.

Large intra- and inter-tumor heterogeneity of OCR measurements were observed within both *time-* and *size-*matched control Calu-6 xenografts. Both types of heterogeneity were markedly reduced in tumors treated with RT (**figure 3E**). In all, 31.3% of control biopsy samples at day 10 (*time-*matched) had OCR of > 25 pmol/ min per normalized unit and this increased to 59.4% in *size-*matched control biopsy samples. In distinction, only 13.0% of RT treated biopsy samples had residual OCR of > 25 pmol/ min per normalized unit. These data provide evidence that the hypoxia modification detected by OE-MRI and pimonidazole immunohistochemistry in Calu-6 is likely due to reduced overall oxygen consumption rate, in particular removing those sub-regions with very high localized oxygen consumption rate.

#### ***Perfused Oxy-R is feasible, well-tolerated and repeatable in NSCLC patients***

Twenty-three stage I-IV NSCLC patients were recruited (**supplementary figure 4; supplementary table 1**). The protocol was safe and well-tolerated (**supplementary table 2**). Significant changes in  $R_1$  were observed following oxygen inhalation in the aorta of all patients demonstrating technique feasibility and providing quality control (**supplementary figure 11**).

Whole tumor median  $R_1$  increased with oxygen inhalation in 11/15 patients (individual all  $p < 0.05$  for 11 patients, oxygen inhalation versus air). However, all tumors demonstrated some degree of intra-tumor spatial heterogeneity in oxygen-induced  $\Delta R_1$ , with three patterns of tissue classification revealed. In 3/15 tumors the whole tumor median  $\Delta R_1$  was significant and had similar temporal evolution and magnitude as the  $\Delta R_1$  seen in the aorta. These tumors had no measurable regional hypoxia (absence of *perfused Oxy-R*; representative example in **figure 4A**). The remaining 12/15 tumors had spatially coherent regions of hypoxia; this included 8/15 tumors with an overall significant  $\Delta R_1$  that was partially attenuated compared with aorta  $\Delta R_1$  (representative example in **figure 4B**), and 4/15 tumors where the proportion of hypoxic tissue was high enough to substantially attenuate the median whole tumor  $\Delta R_1$  so that it was not significant (representative example in **figure 4C**).

Ten patients underwent repeat MRI (within  $7 \pm 5$  days; **supplementary figure 4**) before radiotherapy was administered to measure biomarker precision. The *perfused Oxy-R* volume, measuring tumor hypoxic volume, demonstrated excellent

repeatability with ICC of 0.961 (95% CI 0.858-0.990) and CoV of 25.880% (**figure 4D**). Additional repeatability results can be found in **supplementary table 3**.

Consistent classification of tumors as either entirely normoxic ( $n=3$ ; *perfused Oxy-R* volume =0) or containing some hypoxia ( $n=7$ ; *perfused Oxy-R* volume >0) was concordant between the two pre-radiotherapy scans. Finally, visual inspection revealed that MRI hypoxia mapping was spatially repeatable in tumor, nodal, and distant metastatic lesions across a range of tumor and hypoxic volumes (**figure 4E**). Collectively, these data demonstrate that OE-MRI can identify and map hypoxia in clinical NSCLC tumors, when sub-regional tissue classification is performed using perfusion data.

### ***Perfused Oxy-R detects therapy-induced changes in hypoxia in NSCLC patients***

Twelve patients were imaged at day  $14\pm 4$  of radiotherapy, in addition to pre-treatment imaging (**supplementary figure 4**). No significant change was detected in tumor volume at this time point ( $p=0.159$ ; **table 1**), but we hypothesized that radiation would induce measurable changes in hypoxia within this window, based on previous clinical PET studies in head and neck cancer and lung cancer (11-13).

The *perfused Oxy-R* volume, indicating hypoxic tumor volume, decreased in the patient cohort from  $4.16\text{ cm}^3$  (95% CI  $0-10.6\text{ cm}^3$ ) at baseline to  $3.23\text{ cm}^3$  (95% CI  $0-9.41\text{ cm}^3$ ) at mid-treatment ( $p=0.015$ ). In distinction, the increase in median  $\Delta R_1$  at day 14 was not significant ( $p=0.097$ ). MRI parameter changes are summarized in **table 1**. These data show that the MRI biomarker *perfused Oxy-R* volume detected reduction in tumor hypoxia in patients with NSCLC consistent with data in the two xenograft models of cancer.

### ***Perfused Oxy-R measurement of hypoxia has implications for personalized therapy***

Previous PET studies have reported variable hypoxia modification in patients with NSCLC and other cancer types (11,27,28). We examined the variation in hypoxia modification in Calu-6 xenografts at day 10. Those xenografts with >50% change in hypoxic volume were designated as exhibiting significant hypoxia modification. While RT treated tumors showed overall reduction in hypoxia, relative to control, a >50% decrease in hypoxic volume was seen in only 9/15 tumors (**figure 5A**). These 'hypoxia modified tumors' had higher perfusion and permeability (denoted by median

DCE-MRI  $IAUC_{60}$ ) at baseline than tumors that did not demonstrate hypoxia modification ( $p=0.035$ ; **figure 5B**).

Similarly, variation was seen in response to (chemo)radiotherapy in the clinical tumors, with 8/12 tumors having a decrease in hypoxic volume >50%. In distinction, two tumors had an increase in hypoxic volume >50% and two tumors showed no change above the 50% threshold (**figure 5C**). Tumors with significant reduction in hypoxia had higher median  $IAUC_{60}$  ( $p=0.011$ ) at baseline than other tumors (**figure 5D**). There was no difference in baseline tumor size or hypoxic volume between the hypoxia 'modified' and non-modified tumors. These data show that OE-MRI can distinguish tumors that demonstrate hypoxia modification following RT from those that have persistent hypoxia.

## DISCUSSION

There is an unmet need to develop non-invasive biomarkers of tumor hypoxia to monitor response for anticancer treatments. This is particularly important for radiotherapy and chemoradiotherapy, as meta-analysis has identified the negative impact of hypoxia detected via imaging, on radiotherapy outcome (29).

Imaging enables repeated whole tumor sampling which overcomes the limitations of tissue-based hypoxia quantification (sub-sampling and single measurement) and biofluid assays (inability to distinguish heterogeneity between different tumors in an individual). Therefore, translational imaging tests could enable patient selection and stratification in trials of combined radiotherapy and hypoxia-targeted therapies (10), to adapt radiotherapy dose intensification, and to monitor emergence of radio-resistant hypoxic cancer cells (14).

Here, we report the first-in-human evidence that *perfused Oxy-R* can identify, map, and quantify change in hypoxia induced by a therapeutic intervention. We chose to evaluate patients with NSCLC as a proof-of-principle study because lung cancer is the leading cause of cancer mortality worldwide (30); around 90% of cases are of the NSCLC subtype (31,32); and tumor hypoxia is associated with poor survival in NSCLC patients (33). Furthermore, radiotherapy plays an important role in the treatment of all stages of NSCLC (34) and imaging biomarkers are attractive in this setting due to limited access to tumor tissue material in radiotherapy-treated patients.

Our bench-to-bedside approach began by testing if OE-MRI biomarkers could detect radiotherapy-induced changes in tumor biology in two xenograft models of NSCLC (Calu-6) and high grade glioma (U87). We showed that OE-MRI, combined with assessment of perfusion, identified and mapped regional differences in hypoxic and normoxic tumor in both models, using immunohistochemistry validation (18,35,36). Next we showed that radiotherapy resulted in significant reduction in *perfused Oxy-R* volume in Calu-6 xenografts after 10 days, relative to control tumors, with both high dose single fraction radiotherapy and a fractionated chemoradiotherapy regimen that more closely mimics clinical therapy. These differences persisted to 18-24 days, indicating that while regrowth occurred eventually in the RT and CRT treated tumors, they had less hypoxic tissue than untreated tumors of a similar size. Our findings were validated by *time-* and *size-*matched immunohistochemical quantification of hypoxia and quantification of oxygen consumption. Confirmatory data were obtained in U87 tumors. In all studies, an OE-MRI biomarker that was sensitive to spatial heterogeneity (37) between hypoxic and non-hypoxic tumor sub-regions – *perfused Oxy-R* – was most closely related to hypoxia on pathology validation and was most sensitive to therapeutic modification of hypoxia.

These data are the first to show that *perfused Oxy-R* can track group differences in hypoxia modification following therapy *in vivo*. Mechanistic insight was provided through analysis of the DCE-MRI data acquired during MRI-treatment experiments in Calu-6 and U87 xenografts showed that increases in tumor perfusion (measured by  $IAUC_{60}$ ) were detected with radiation based therapies, relative to control. Further, *ex vivo* OCR analysis in Calu-6 xenografts provided evidence that oxygen consumption was reduced at day 10 following RT. These data suggests that both increased oxygen delivery and reduced oxygen consumption contribute to radiation-induced hypoxia modification.

We then translated the OE-MRI technique to humans, demonstrating safety, tolerability, and measurement feasibility in NSCLC patients. Measurement precision was evaluated by assessing biomarker repeatability. *Perfused Oxy-R* (hypoxic) volume had excellent test-retest precision with high ICC and compared favorably with previously published studies of MRI biomarker precision in lung and other tumors (38-41). The intra-tumor spatial distribution of hypoxia was comparable between repeat scans on visual inspection. Lack of absolute visual repeatability could be due to methodological factors (including imperfect image registration or inconsistent

target volume definition) or biological factors (including cyclical hypoxia) (14). Further, OE-MRI provided consistent classification of tumors as hypoxic or not; in this respect it outperformed PET imaging with the tracer [<sup>18</sup>F]FMISO in patients with NSCLC (42). These data are the first to demonstrate repeatability of OE-MRI biomarkers that quantify tumor hypoxia in patients with cancer.

Our clinical data provides the first evidence that OE-MRI can track tumor hypoxia modification induced by a therapy in patients. This finding concurs with previous PET imaging studies in patients with NSCLC and other cancers which have shown that the volume of hypoxic tumor can increase, decrease or remain unchanged within the initial few weeks following chemoradiation (11).

Finally, since PET studies in patients with head and neck cancer suggest that the persistence of hypoxia during chemoradiotherapy, rather than pretreatment levels of hypoxia, predict clinical outcome (12,13), we investigated the potential for OE-MRI to have application in personalized medicine. We demonstrated that *perfused Oxy-R* distinguished those xenografts and NSCLC patient tumors whose hypoxic tumor volume decreases following radiotherapy-based treatments from those that remained hypoxic (and in some cases worsened). Of note, hypoxia modification was observed in tumors with relatively high pretreatment vascular perfusion and permeability, measured by *IAUC<sub>60</sub>*. This suggests that a multimodal imaging, genomic and tissue pathology biomarker panel – performed before and during treatment – may be required to fully understand, predict and monitor hypoxia modification in the clinic (43). However, further prospective powered studies are required to confirm any role for hypoxia imaging in stratified medicine.

While this study focused on the role of *perfused Oxy-R* in measuring hypoxia changes induced by radiotherapy, these findings have broad implications. *Perfused Oxy-R* has potential to monitor direct pharmacological targeting of hypoxia (44) and to inform how resistance to immunotherapy relates to the hypoxic tumor stem cell niche (9). Further, *perfused Oxy-R* may guide radiotherapy dose intensification (dose painting) (45,46) and has unique potential for clinical applications such as real-time adaptive radiotherapy on MR Linac systems (47). For each of these applications, large studies are required to qualify the prognostic value of *perfused Oxy-R* as a biomarker of hypoxia and its ability to predict therapy response.

In summary, this study provides substantial new information to advance clinical translation of the OE-MRI and DCE-MRI biomarker *perfused Oxy-R* volume (48) and supports further effort to qualify this biomarker for use in clinical trials.

## REFERENCES

1. Brizel DM, Sibley GS, Prosnitz LR, Scher RL, Dewhirst MW. Tumor hypoxia adversely affects the prognosis of carcinoma of the head and neck. *International journal of radiation oncology, biology, physics* **1997**;38(2):285-9.
2. Hockel M, Schlenger K, Aral B, Mitze M, Schaffer U, Vaupel P. Association between tumor hypoxia and malignant progression in advanced cancer of the uterine cervix. *Cancer research* **1996**;56(19):4509-15.
3. Vergis R, Corbishley CM, Norman AR, Bartlett J, Jhavar S, Borre M, *et al.* Intrinsic markers of tumour hypoxia and angiogenesis in localised prostate cancer and outcome of radical treatment: a retrospective analysis of two randomised radiotherapy trials and one surgical cohort study. *The Lancet Oncology* **2008**;9(4):342-51 doi 10.1016/s1470-2045(08)70076-7.
4. Yang L, Taylor J, Eustace A, Irlam JJ, Denley H, Hoskin PJ, *et al.* A Gene Signature for Selecting Benefit from Hypoxia Modification of Radiotherapy for High-Risk Bladder Cancer Patients. *Clinical cancer research : an official journal of the American Association for Cancer Research* **2017**;23(16):4761-8 doi 10.1158/1078-0432.ccr-17-0038.
5. Holden SA, Teicher BA, Ara G, Herman TS, Coleman CN. Enhancement of alkylating agent activity by SR-4233 in the FSaIIc murine fibrosarcoma. *Journal of the National Cancer Institute* **1992**;84(3):187-93.
6. Overgaard J. Hypoxic radiosensitization: adored and ignored. *Journal of clinical oncology : official journal of the American Society of Clinical Oncology* **2007**;25(26):4066-74 doi 10.1200/jco.2007.12.7878.
7. Vaupel P, Mayer A. Hypoxia in cancer: significance and impact on clinical outcome. *Cancer metastasis reviews* **2007**;26(2):225-39 doi 10.1007/s10555-007-9055-1.
8. Lin SH, Koong AC. Breathing New Life Into Hypoxia-Targeted Therapies for Non-Small Cell Lung Cancer. *Journal of the National Cancer Institute* **2018**;110(1) doi 10.1093/jnci/djx163.
9. Taylor CT, Colgan SP. Regulation of immunity and inflammation by hypoxia in immunological niches. *Nature reviews Immunology* **2017**;17(12):774-85 doi 10.1038/nri.2017.103.
10. Wilson WR, Hay MP. Targeting hypoxia in cancer therapy. *Nature reviews Cancer* **2011**;11(6):393-410 doi 10.1038/nrc3064.
11. Bollineni VR, Koole MJ, Pruijm J, Brouwer CL, Wiegman EM, Groen HJ, *et al.* Dynamics of tumor hypoxia assessed by 18F-FAZA PET/CT in head and neck and lung cancer patients during chemoradiation: possible implications for radiotherapy treatment planning strategies. *Radiotherapy and oncology : journal of the European Society for Therapeutic Radiology and Oncology* **2014**;113(2):198-203 doi 10.1016/j.radonc.2014.10.010.
12. Lock S, Perrin R, Seidlitz A, Bandurska-Luque A, Zschaeck S, Zophel K, *et al.* Residual tumour hypoxia in head-and-neck cancer patients undergoing primary radiochemotherapy, final results of a prospective trial on repeat FMISO-PET imaging. *Radiotherapy and oncology : journal of the European Society for Therapeutic Radiology and Oncology* **2017**;124(3):533-40 doi 10.1016/j.radonc.2017.08.010.
13. Zips D, Zophel K, Abolmaali N, Perrin R, Abramyuk A, Haase R, *et al.* Exploratory prospective trial of hypoxia-specific PET imaging during radiochemotherapy in patients with locally advanced head-and-neck cancer. *Radiotherapy and oncology : journal of the European Society for Therapeutic Radiology and Oncology* **2012**;105(1):21-8 doi 10.1016/j.radonc.2012.08.019.
14. Salem A, Asselin MC, Reymen B, Jackson A, Lambin P, West CML, *et al.* Targeting Hypoxia to Improve Non-Small Cell Lung Cancer Outcome. *Journal of the National Cancer Institute* **2018**;110(1):14-30 doi 10.1093/jnci/djx160.
15. Young IR, Clarke GJ, Bailes DR, Pennock JM, Doyle FH, Bydder GM. Enhancement of relaxation rate with paramagnetic contrast agents in NMR imaging. *The Journal of computed tomography* **1981**;5(6):543-7.
16. Dewhirst MW, Brier SR. Oxygen-Enhanced MRI Is a Major Advance in Tumor Hypoxia Imaging. *Cancer research* **2016**;76(4):769-72 doi 10.1158/0008-5472.can-15-2818.

17. Workman P, Aboagye EO, Balkwill F, Balmain A, Bruder G, Chaplin DJ, *et al.* Guidelines for the welfare and use of animals in cancer research. *British journal of cancer* **2010**;102(11):1555-77 doi 10.1038/sj.bjc.6605642.
18. O'Connor JP, Boulton JK, Jamin Y, Babur M, Finegan KG, Williams KJ, *et al.* Oxygen-Enhanced MRI Accurately Identifies, Quantifies, and Maps Tumor Hypoxia in Preclinical Cancer Models. *Cancer research* **2016**;76(4):787-95 doi 10.1158/0008-5472.CAN-15-2062.
19. Russell S, Wojtkowiak J, Neilson A, Gillies RJ. Metabolic Profiling of healthy and cancerous tissues in 2D and 3D. *Scientific reports* **2017**;7(1):15285 doi 10.1038/s41598-017-15325-5.
20. Tofts PS, Brix G, Buckley DL, Evelhoch JL, Henderson E, Knopp MV, *et al.* Estimating kinetic parameters from dynamic contrast-enhanced T(1)-weighted MRI of a diffusible tracer: standardized quantities and symbols. *Journal of magnetic resonance imaging : JMRI* **1999**;10(3):223-32.
21. O'Connor JP, Jackson A, Parker GJ, Roberts C, Jayson GC. Dynamic contrast-enhanced MRI in clinical trials of antivasculature therapies. *Nature reviews Clinical oncology* **2012**;9(3):167-77 doi 10.1038/nrclinonc.2012.2.
22. Portney LG, Watkins MP. *Foundations of clinical research: applications to practice.* Prentice Hall; 2000.
23. Williams KJ, Telfer BA, Shannon AM, Babur M, Stratford IJ, Wedge SR. Combining radiotherapy with AZD2171, a potent inhibitor of vascular endothelial growth factor signaling: pathophysiologic effects and therapeutic benefit. *Molecular cancer therapeutics* **2007**;6(2):599-606 doi 10.1158/1535-7163.mct-06-0508.
24. Jiang Y, Verbiest T, Devery AM, Bokobza SM, Weber AM, Leszczynska KB, *et al.* Hypoxia Potentiates the Radiation-Sensitizing Effect of Olaparib in Human Non-Small Cell Lung Cancer Xenografts by Contextual Synthetic Lethality. *International journal of radiation oncology, biology, physics* **2016**;95(2):772-81 doi 10.1016/j.ijrobp.2016.01.035.
25. Joseph JV, Conroy S, Pavlov K, Sontakke P, Tomar T, Eggens-Meijer E, *et al.* Hypoxia enhances migration and invasion in glioblastoma by promoting a mesenchymal shift mediated by the HIF1alpha-ZEB1 axis. *Cancer letters* **2015**;359(1):107-16 doi 10.1016/j.canlet.2015.01.010.
26. Matsumoto K, Bernardo M, Subramanian S, Choyke P, Mitchell JB, Krishna MC, *et al.* MR assessment of changes of tumor in response to hyperbaric oxygen treatment. *Magnetic resonance in medicine : official journal of the Society of Magnetic Resonance in Medicine / Society of Magnetic Resonance in Medicine* **2006**;56(2):240-6 doi 10.1002/mrm.20961.
27. Koh WJ, Bergman KS, Rasey JS, Peterson LM, Evans ML, Graham MM, *et al.* Evaluation of oxygenation status during fractionated radiotherapy in human nonsmall cell lung cancers using [F-18]fluoromisonidazole positron emission tomography. *International journal of radiation oncology, biology, physics* **1995**;33(2):391-8 doi 10.1016/0360-3016(95)00170-4.
28. Vera P, Bohn P, Edet-Sanson A, Salles A, Hapdey S, Gardin I, *et al.* Simultaneous positron emission tomography (PET) assessment of metabolism with (1)(8)F-fluoro-2-deoxy-d-glucose (FDG), proliferation with (1)(8)F-fluoro-thymidine (FLT), and hypoxia with (1)(8)fluoro-misonidazole (F-miso) before and during radiotherapy in patients with non-small-cell lung cancer (NSCLC): a pilot study. *Radiotherapy and oncology : journal of the European Society for Therapeutic Radiology and Oncology* **2011**;98(1):109-16 doi 10.1016/j.radonc.2010.10.011.
29. Horsman MR, Mortensen LS, Petersen JB, Busk M, Overgaard J. Imaging hypoxia to improve radiotherapy outcome. *Nature reviews Clinical oncology* **2012**;9(12):674-87 doi 10.1038/nrclinonc.2012.171.
30. Jemal A, Bray F, Center MM, Ferlay J, Ward E, Forman D. Global cancer statistics. *CA: a cancer journal for clinicians* **2011**;61(2):69-90 doi 10.3322/caac.20107.
31. Govindan R, Page N, Morgensztern D, Read W, Tierney R, Vlahiotis A, *et al.* Changing epidemiology of small-cell lung cancer in the United States over the last 30 years: analysis of the surveillance, epidemiologic, and end results database. *Journal of clinical oncology : official journal of the American Society of Clinical Oncology* **2006**;24(28):4539-44 doi 10.1200/jco.2005.04.4859.

32. Riaz SP, Luchtenborg M, Coupland VH, Spicer J, Peake MD, Moller H. Trends in incidence of small cell lung cancer and all lung cancer. *Lung cancer* **2012**;75(3):280-4 doi 10.1016/j.lungcan.2011.08.004.
33. Wang Q, Hu DF, Rui Y, Jiang AB, Liu ZL, Huang LN. Prognosis value of HIF-1alpha expression in patients with non-small cell lung cancer. *Gene* **2014**;541(2):69-74 doi 10.1016/j.gene.2014.03.025.
34. Johnson DH, Schiller JH, Bunn PA, Jr. Recent clinical advances in lung cancer management. *Journal of clinical oncology : official journal of the American Society of Clinical Oncology* **2014**;32(10):973-82 doi 10.1200/jco.2013.53.1228.
35. Linnik IV, Scott ML, Holliday KF, Woodhouse N, Waterton JC, O'Connor JP, *et al.* Noninvasive tumor hypoxia measurement using magnetic resonance imaging in murine U87 glioma xenografts and in patients with glioblastoma. *Magnetic resonance in medicine : official journal of the Society of Magnetic Resonance in Medicine / Society of Magnetic Resonance in Medicine* **2014**;71(5):1854-62 doi 10.1002/mrm.24826.
36. Little R, Jamin Y, Boulton J, Naish J, Watson Y, Cheung S, *et al.* Combined oxygen and gadolinium enhanced MR imaging of hypoxia in renal carcinoma: comparison with susceptibility MR imaging and pathology. *Radiology* **2018**;288:739-47.
37. O'Connor JP, Rose CJ, Waterton JC, Carano RA, Parker GJ, Jackson A. Imaging intratumor heterogeneity: role in therapy response, resistance, and clinical outcome. *Clinical cancer research : an official journal of the American Association for Cancer Research* **2015**;21(2):249-57 doi 10.1158/1078-0432.ccr-14-0990.
38. Morgan B, Utting JF, Higginson A, Thomas AL, Steward WP, Horsfield MA. A simple, reproducible method for monitoring the treatment of tumours using dynamic contrast-enhanced MR imaging. *British journal of cancer* **2006**;94(10):1420-7 doi 10.1038/sj.bjc.6603140.
39. Ng CS, Raunig DL, Jackson EF, Ashton EA, Kelcz F, Kim KB, *et al.* Reproducibility of perfusion parameters in dynamic contrast-enhanced MRI of lung and liver tumors: effect on estimates of patient sample size in clinical trials and on individual patient responses. *AJR American journal of roentgenology* **2010**;194(2):W134-40 doi 10.2214/ajr.09.3116.
40. O'Connor JP, Carano RA, Clamp AR, Ross J, Ho CC, Jackson A, *et al.* Quantifying antivascular effects of monoclonal antibodies to vascular endothelial growth factor: insights from imaging. *Clinical cancer research : an official journal of the American Association for Cancer Research* **2009**;15(21):6674-82 doi 10.1158/1078-0432.ccr-09-0731.
41. Weller A, Papoutsaki MV, Waterton JC, Chiti A, Stroobants S, Kuijter J, *et al.* Diffusion-weighted (DW) MRI in lung cancers: ADC test-retest repeatability. *European radiology* **2017**;27(11):4552-62 doi 10.1007/s00330-017-4828-6.
42. Grkovski M, Schwartz J, Rimmer A, Schoder H, Carlin SD, Zanzonico PB, *et al.* Reproducibility of 18F-fluoromisonidazole intratumour distribution in non-small cell lung cancer. *EJNMMI research* **2016**;6(1):79 doi 10.1186/s13550-016-0210-y.
43. Lalonde E, Ishkanian AS, Sykes J, Fraser M, Ross-Adams H, Erho N, *et al.* Tumour genomic and microenvironmental heterogeneity for integrated prediction of 5-year biochemical recurrence of prostate cancer: a retrospective cohort study. *The Lancet Oncology* **2014**;15(13):1521-32 doi 10.1016/s1470-2045(14)71021-6.
44. Tap WD, Papai Z, Van Tine BA, Attia S, Ganjoo KN, Jones RL, *et al.* Doxorubicin plus evofosfamide versus doxorubicin alone in locally advanced, unresectable or metastatic soft-tissue sarcoma (TH CR-406/SARC021): an international, multicentre, open-label, randomised phase 3 trial. *The Lancet Oncology* **2017**;18(8):1089-103 doi 10.1016/s1470-2045(17)30381-9.
45. Vera P, Thureau S, Chaumet-Riffaud P, Modzelewski R, Bohn P, Vermandel M, *et al.* Phase II Study of a Radiotherapy Total Dose Increase in Hypoxic Lesions Identified by 18F-Misonidazole PET/CT in Patients with Non-Small Cell Lung Carcinoma (RTEP5 Study). *Journal of nuclear medicine : official publication, Society of Nuclear Medicine* **2017**;58(7):1045-53 doi 10.2967/jnumed.116.188367.
46. van Elmpt W, De Ruyscher D, van der Salm A, Lakeman A, van der Stoep J, Emans D, *et al.* The PET-boost randomised phase II dose-escalation trial in non-small cell lung cancer. *Radiotherapy and oncology : journal of the European Society for*

- Therapeutic Radiology and Oncology **2012**;104(1):67-71 doi 10.1016/j.radonc.2012.03.005.
47. Bainbridge H, Salem A, Tijssen RHN, Dubec M, Wetscherek A, Van Es C, *et al.* Magnetic resonance imaging in precision radiation therapy for lung cancer. Translational lung cancer research **2017**;6(6):689-707 doi 10.21037/tlcr.2017.09.02.
  48. O'Connor JP, Aboagye EO, Adams JE, Aerts HJ, Barrington SF, Beer AJ, *et al.* Imaging biomarker roadmap for cancer studies. Nature reviews Clinical oncology **2017**;14(3):169-86 doi 10.1038/nrclinonc.2016.162.

**Table 1:** Baseline and mid-treatment imaging parameters in patients with NSCLC

<b>Parameter (unit)</b>	<b>Baseline (95% CI)</b>	<b>Mid-treatment (95% CI)</b>	<b>p-value</b>
Tumor volume (cm <sup>3</sup> )	36.7 (9.40-640)	31.7 (5.90-57.6)	0.159
<i>Perfused Oxy-R</i> volume (cm <sup>3</sup> )	4.16 (0-10.60)	3.230 (0-9.410)	<b>0.015</b>
$\Delta R_1$ (s <sup>-1</sup> )	0.018 (0.013-0.023)	0.025 (0.016-0.033)	0.097

## FIGURE LEGENDS

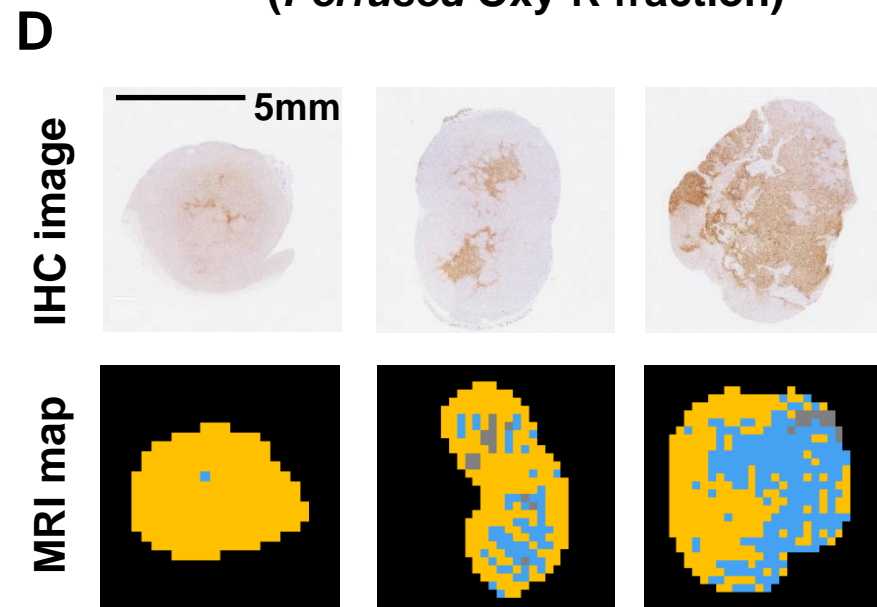
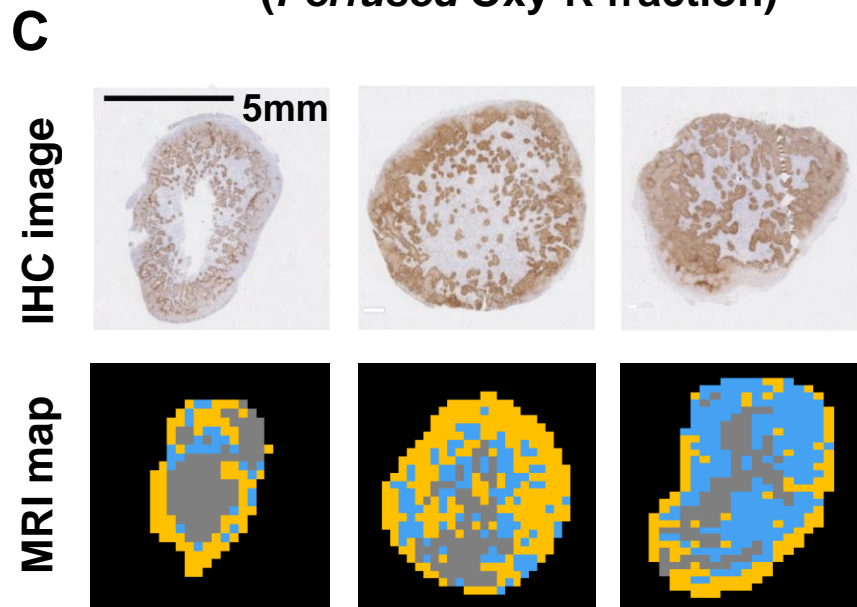
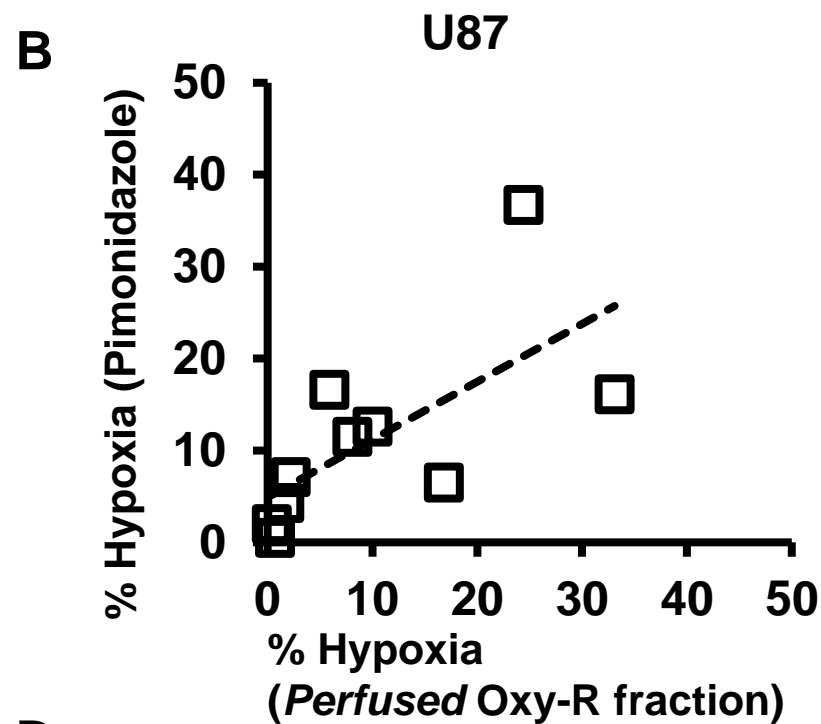
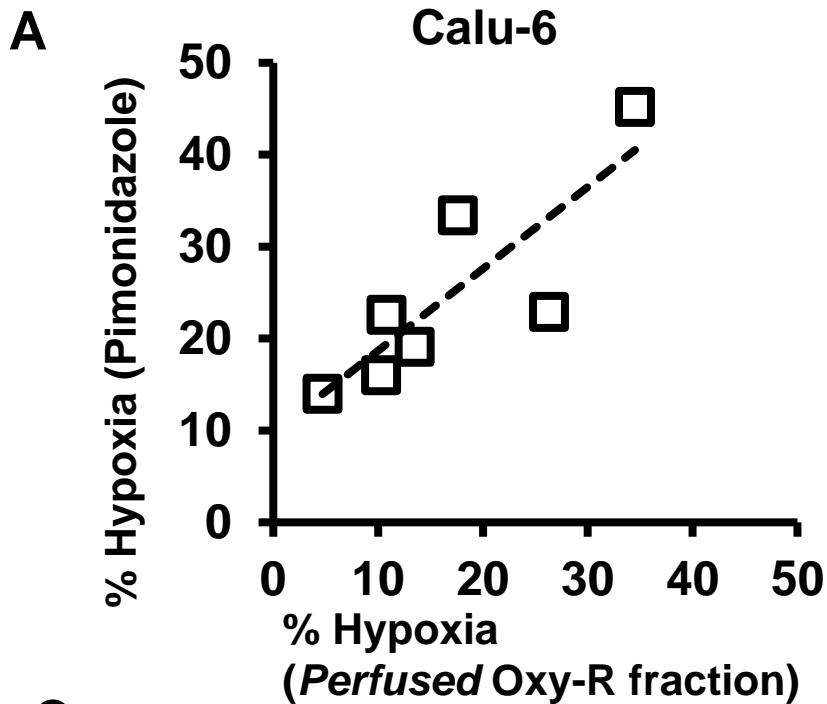
**Figure 1:** The MRI *perfused Oxy-R* fraction correlated with pimonidazole immunohistochemistry derived hypoxic fraction in both untreated (A) Calu-6 tumors and (B) U87 tumors. Example whole field pimonidazole immunohistochemistry and MRI *perfused Oxy-R* maps are shown for the least hypoxic, middle and most hypoxic (C) Calu-6 tumors and (D) U87 tumors.

**Figure 2:** (A) Radiotherapy induced significant growth delay in Calu-6 xenografts treated with single fraction 10 Gy and fractionated 5 x 2 Gy with concurrent cisplatin, relative to control. Tumor measurements were by calipers, with day 0 being the first day of MRI. (B) Mean *perfused Oxy-R* volume was reduced in both radiotherapy treated groups at day 10, relative to control tumors, and this reduction persisted until day 18 (chemoradiotherapy) or day 25 (radiotherapy). (C) Example maps of *perfused Oxy-E* (normoxic tumor), *perfused Oxy-R* (hypoxic tumor) and non-perfused tumor for each treatment group. (D) *Time*-matched data from pimonidazole adduct formation immunohistochemistry staining obtained at day 10 in an independent cohort showed relatively lower hypoxic fraction in radiotherapy treated Calu-6 xenografts relative to control. (E) Pimonidazole adduct formation immunohistochemistry data acquired from the xenografts imaged with MRI confirmed persistent reduction in hypoxic fraction at *size*-matched tumor harvest, with (F) corresponding sample images (magnification 20X). \*\* indicates  $p < 0.001$  and \* indicates  $p < 0.05$ .

**Figure 3:** (A) Oxygen delivery (indicated by the perfusion biomarker  $IAUC_{60}$ ) was increased significantly at days 6-10 in Calu-6 xenografts treated with either RT or CRT, relative to control. (B) Representative maps in one mice from each cohort. (C) Oxygen consumption rate (OCR) was significantly reduced in radiotherapy treated Calu-6 tumors relative to in *time*-matched and *size*-matched controls. Mean OCR values of each tumor (6 samples per tumor) over 5 real-time measurements are shown. (D) There was no difference in biopsy sample necrosis in any of the three groups. (E) Significant intra-tumor and inter-tumor heterogeneity in OCR was observed within *time*- and *size*-matched control Calu-6 xenografts, but this was markedly reduced in tumors treated with radiotherapy. Individual symbols representative different tumors. Error bars are standard error of the mean in all panels. \*\* indicates  $p < 0.001$  and \* indicates  $p < 0.05$ .

**Figure 4:** Three distinct patterns of tissue classification were seen on MRI. In each row, aortic input functions and whole tumor OE-MRI  $\Delta R_1$  were derived from the same patient. **(A)** In 3/15 tumors whole tumor median OE-MRI  $\Delta R_1$  had similar temporal evolution and magnitude as aortic  $\Delta R_1$ ; these tumors had no measurable regional hypoxia (absence of *perfused Oxy-R*). Representative tumor displaying this distinct pattern of tissue classification is shown. **(B)** In 8/15 tumors whole tumor median OE-MRI  $\Delta R_1$ , was partially attenuated by hypoxic regions, but was still significant. Representative tumor displaying this distinct pattern of tissue classification is shown. **(C)** In 4/15 tumors the extent of hypoxia substantially attenuated the whole tumor  $\Delta R_1$  which was not significantly different from zero change. Representative tumor displaying this distinct pattern of tissue classification is shown. **(D)** Bland-Altman plot for *perfused Oxy-R* volume with upper and lower limit of agreement (LoA). Tumor, nodal and distant metastatic lesions are indicated. **(E)** MRI mapping of tumor hypoxia was spatially repeatable to varying extents in tumor, nodal and distant metastatic lesions across a range of tumor and hypoxic volumes.

**Figure 5:** **(A)** Waterfall plot data show that *perfused Oxy-R* volume quantified the variation in hypoxia modification in radiotherapy and fractionated chemoradiotherapy treated Calu-6 xenografts at day 10 and in controls. **(B)** We found that 'modified tumors' had higher perfusion and permeability (denoted by median  $IAUC_{60}$ ) at baseline than tumors that did not demonstrate hypoxia modification (non-responders). Example  $IAUC_{60}$  maps from 'modified' and non-modified tumors shown. **(C)** Waterfall plot data shows that *perfused Oxy-R* volume also quantified the variation in the 12 NSCLC patients receiving (chemo)radiotherapy. Overall there was a significant reduction in hypoxia in this cohort. **(D)** Inter-tumor heterogeneity was also seen here with 'modified tumors' having higher median  $IAUC_{60}$ . Error bars are standard error of the mean. \* indicates  $p < 0.05$ .

**FIGURE 1**

■ *Perfused Oxy-E* (normoxia)

■ *Perfused Oxy-R* (hypoxia)

■ Non-perfused

**FIGURE 2**

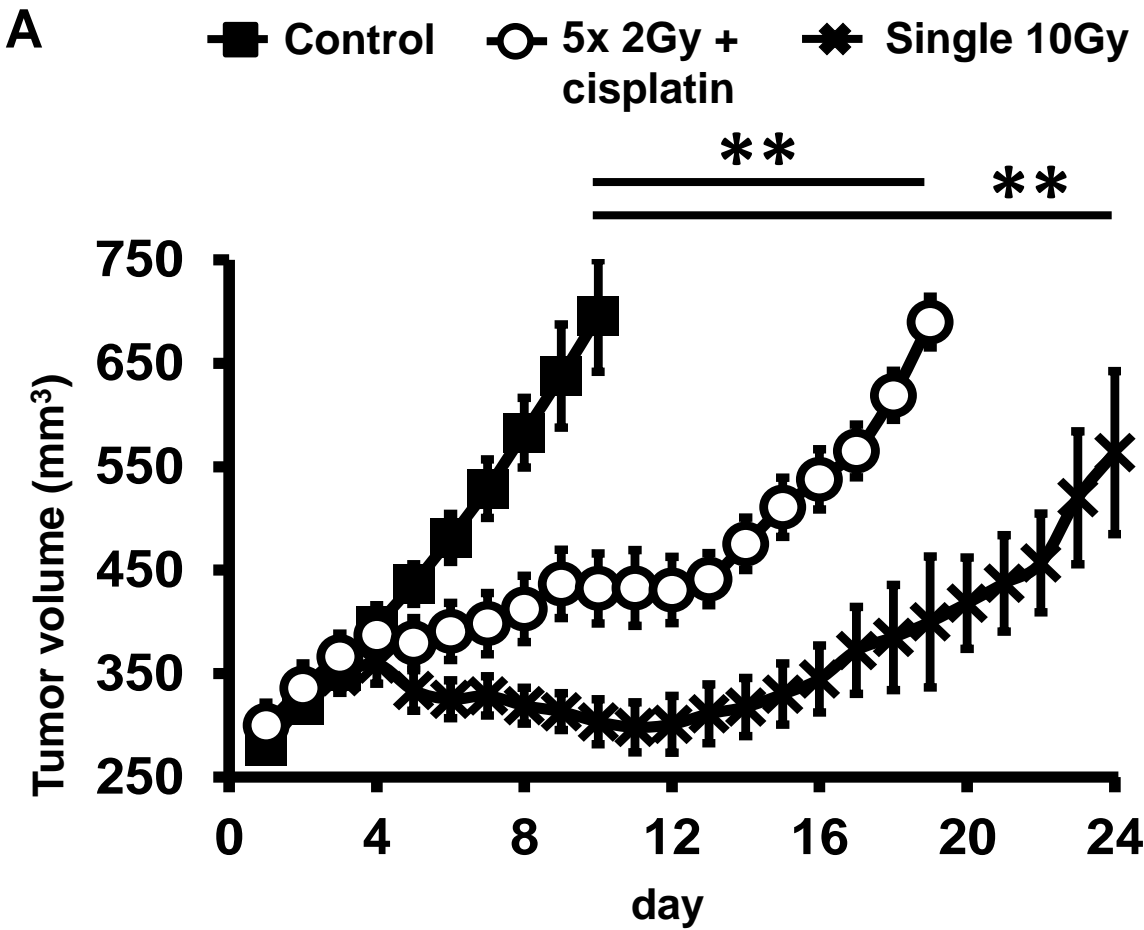


**FIGURE 2**

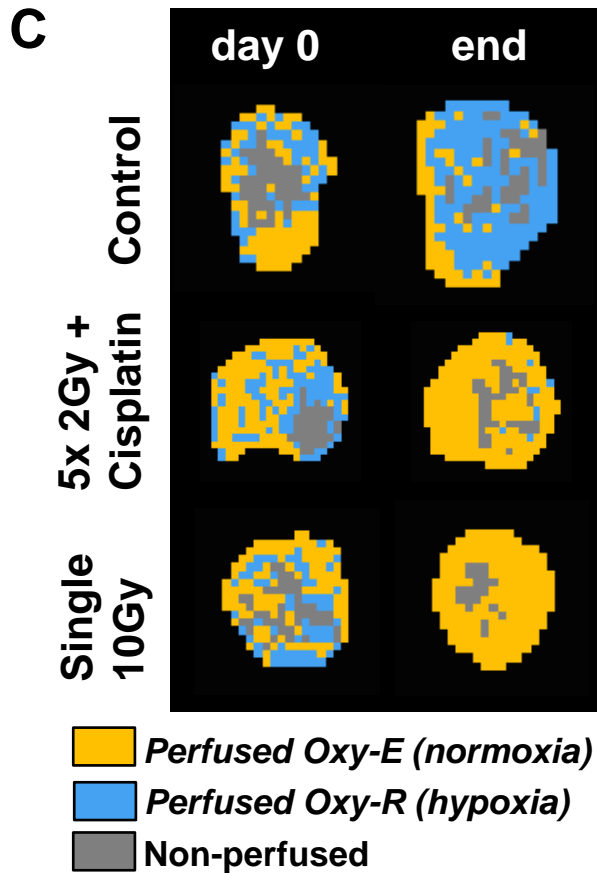
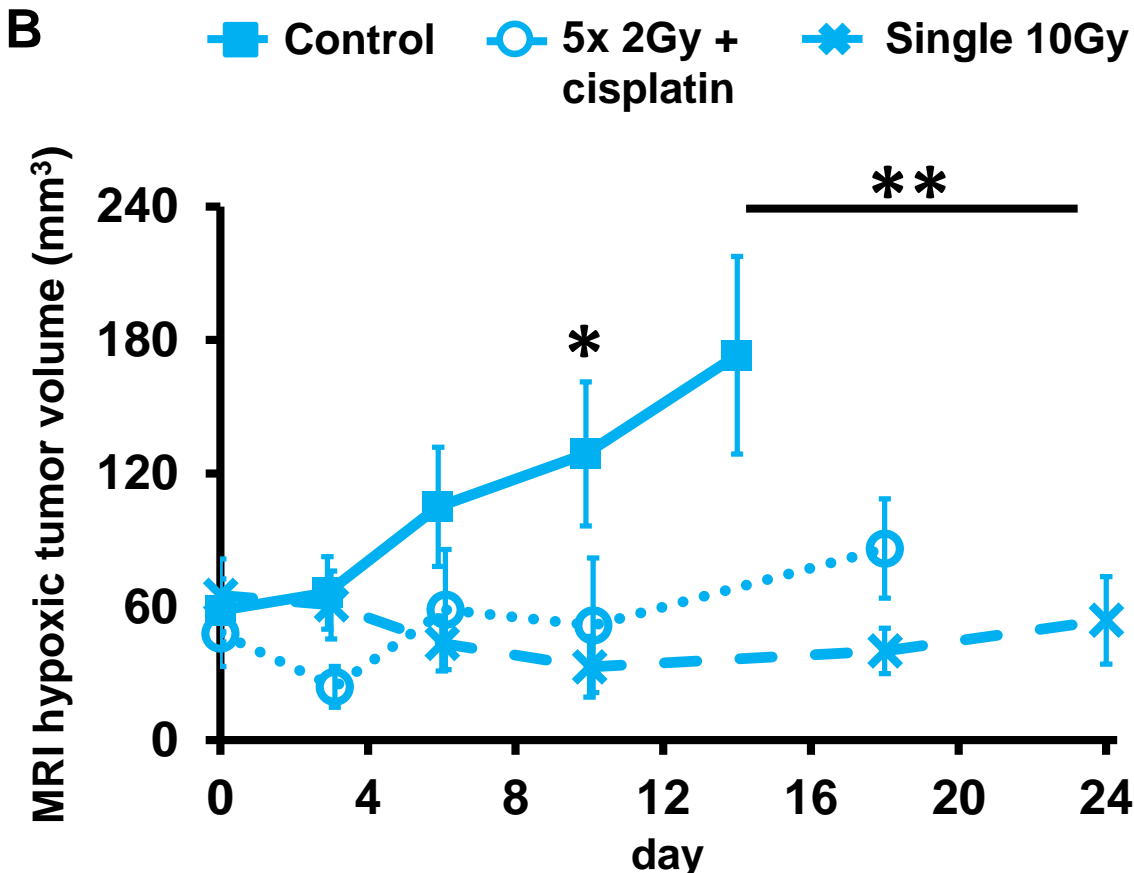


**FIGURE 2**

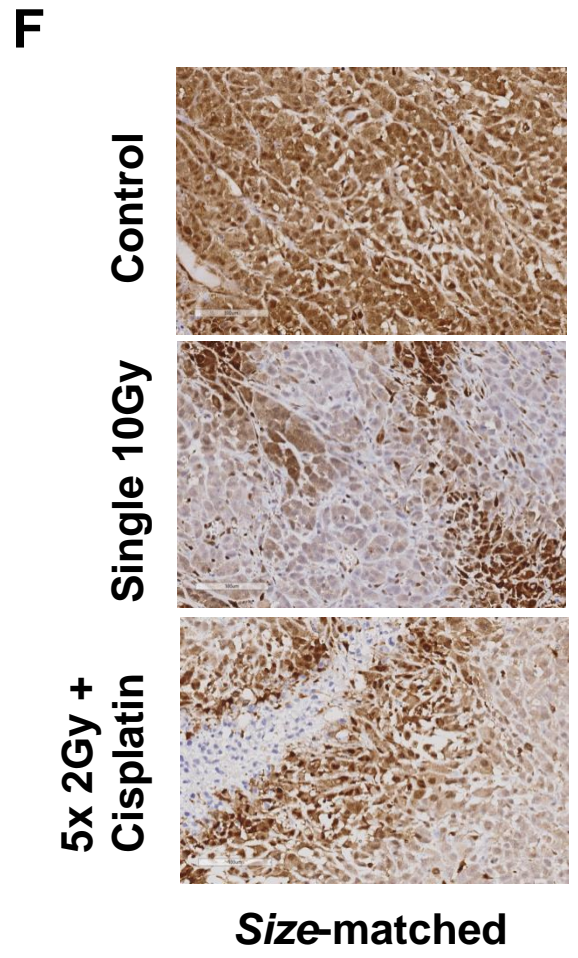
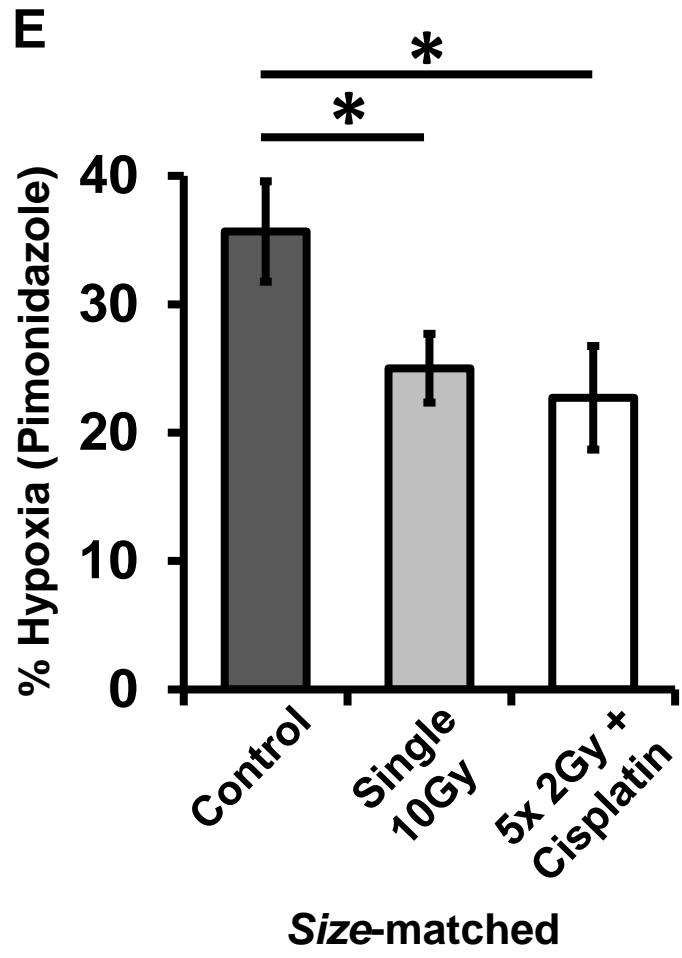
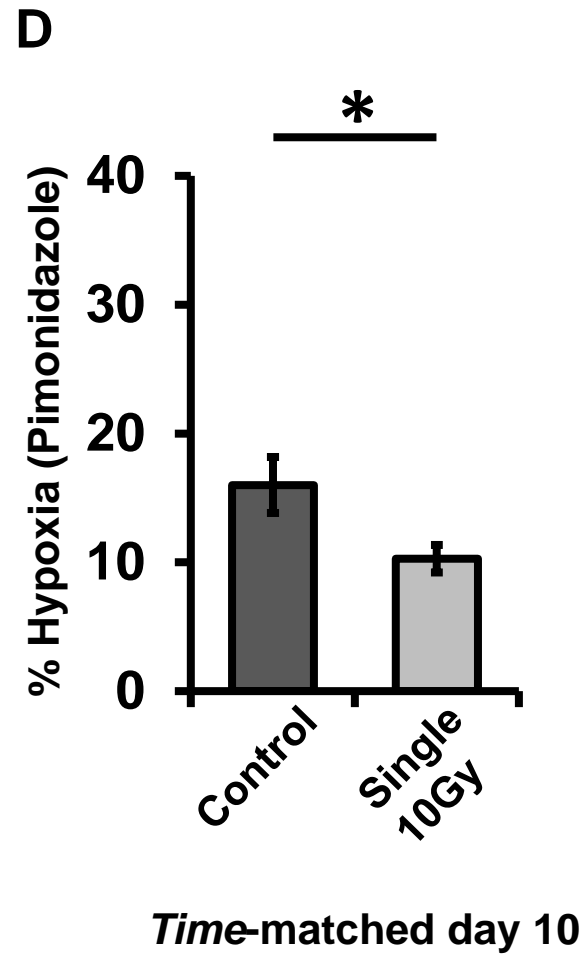
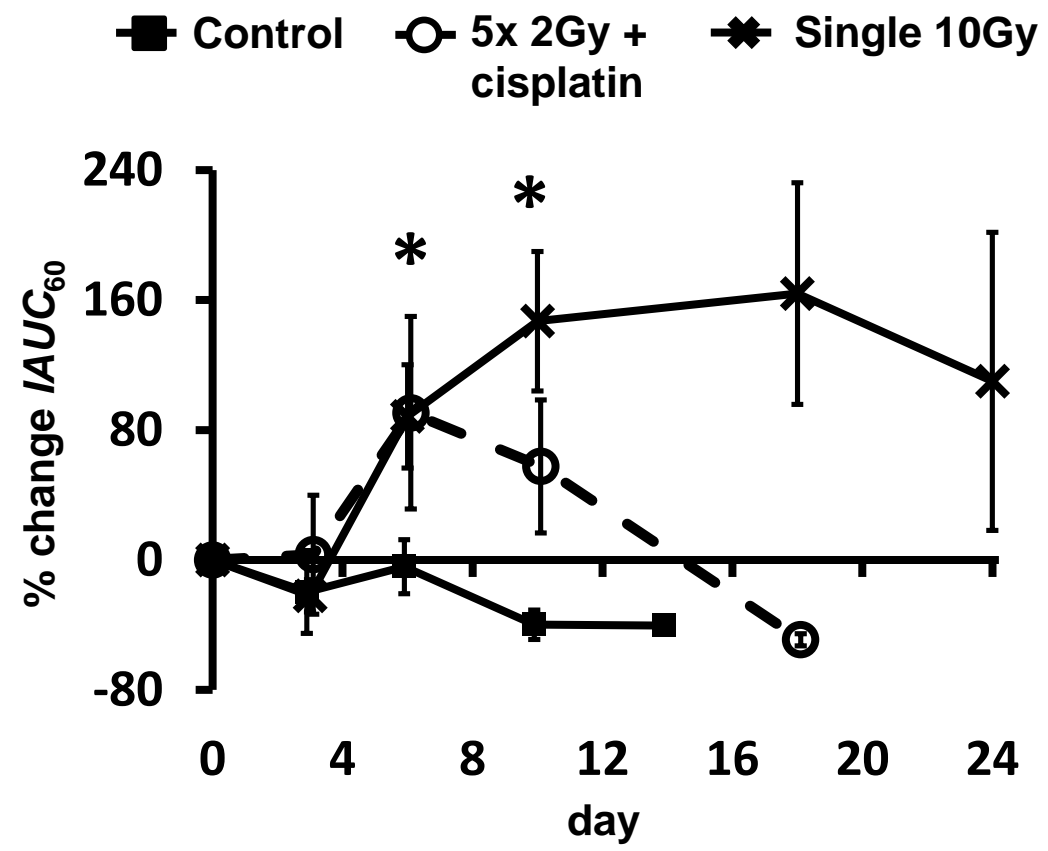
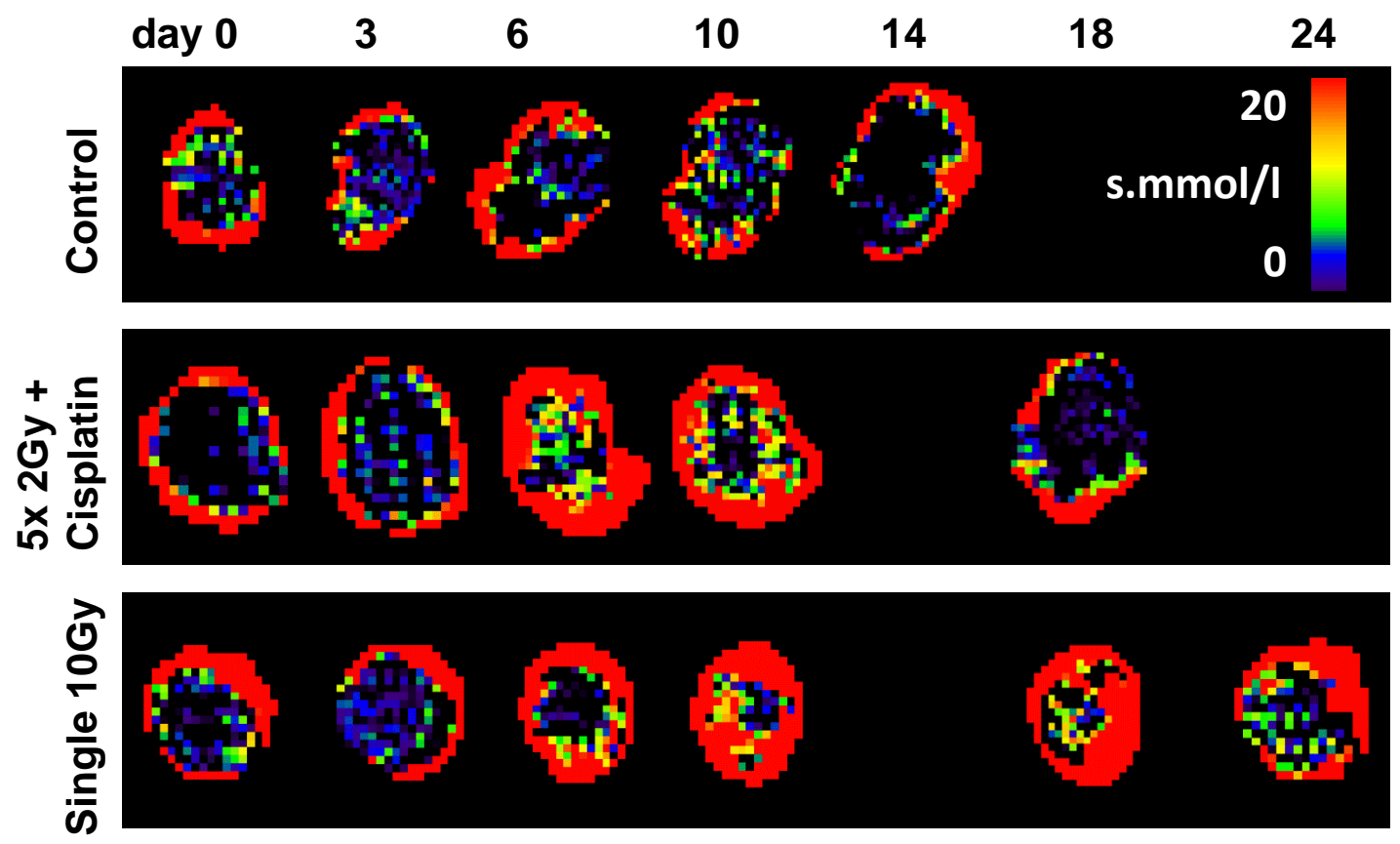


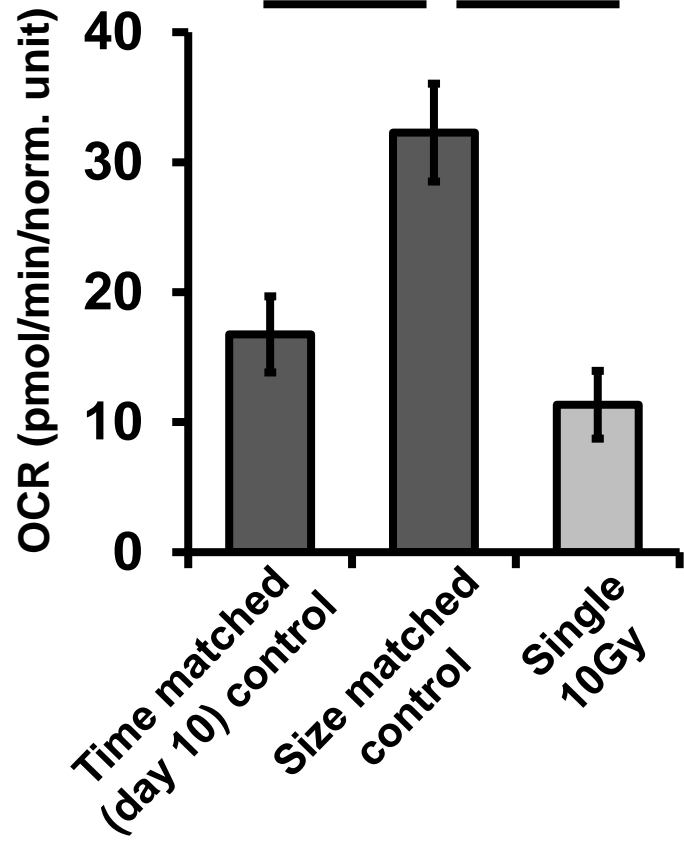
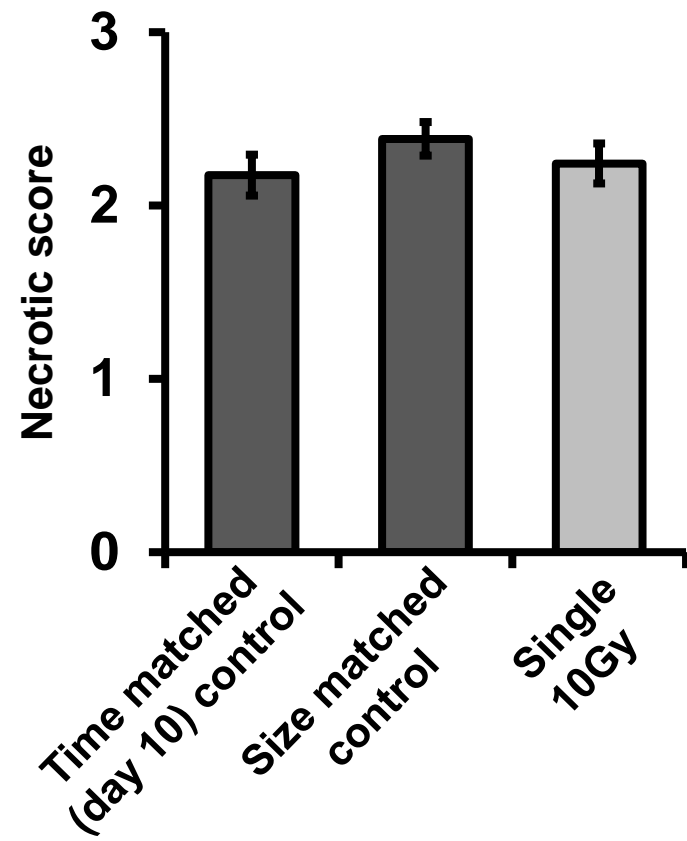
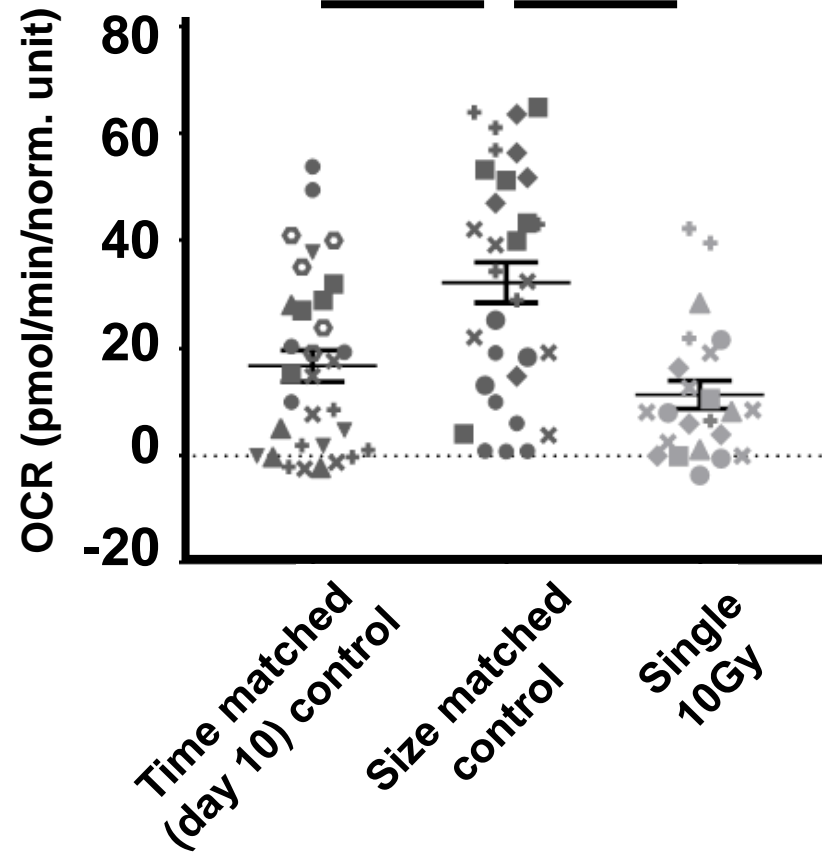
**FIGURE 3**

**A**



**B**



**C****D****E**

**FIGURE 4**

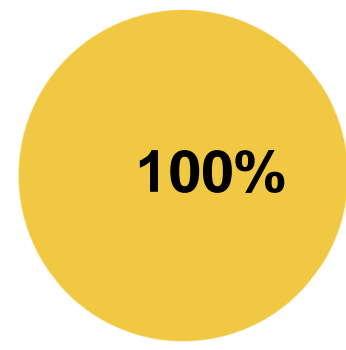
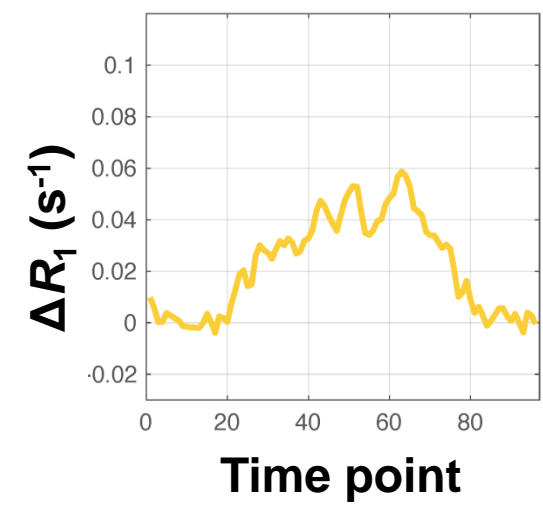
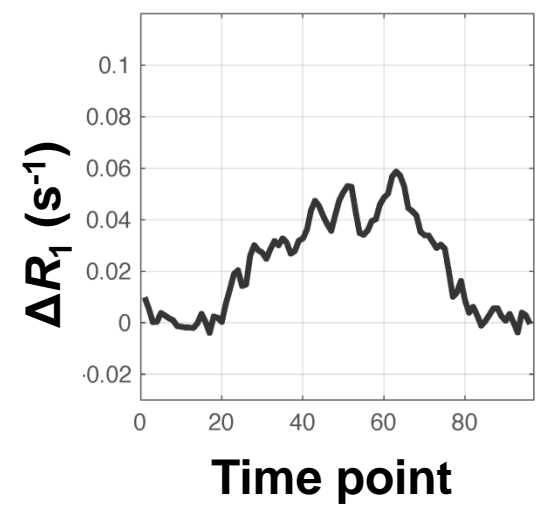
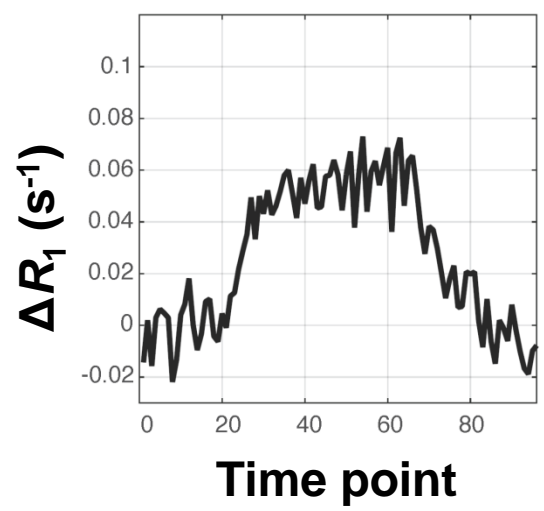
**Aorta input function**

**Whole tumor  $\Delta R_1$**

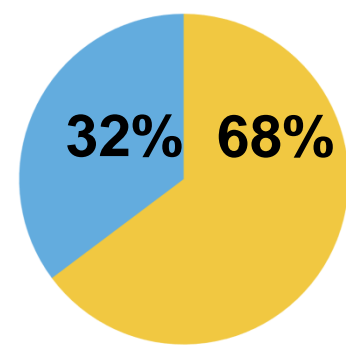
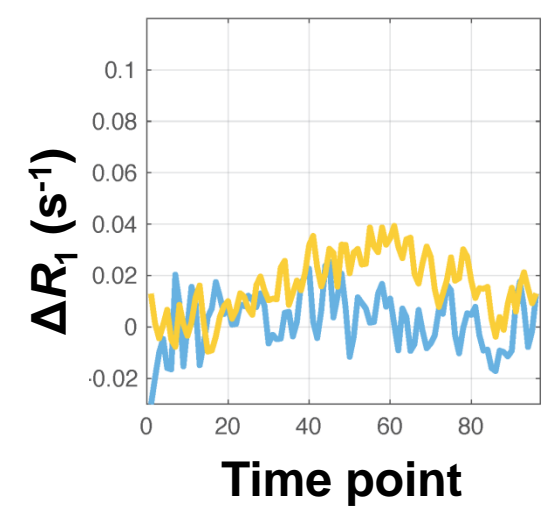
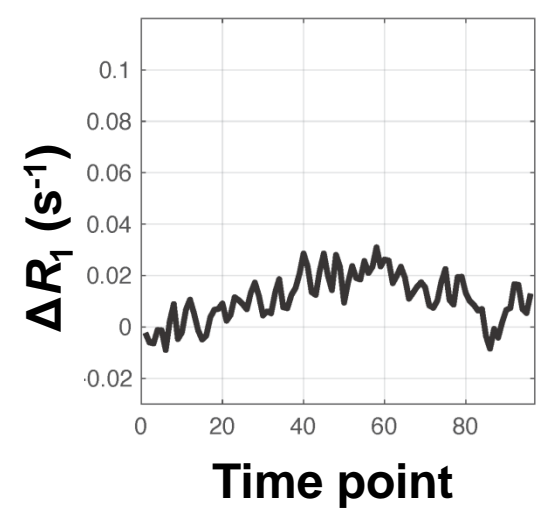
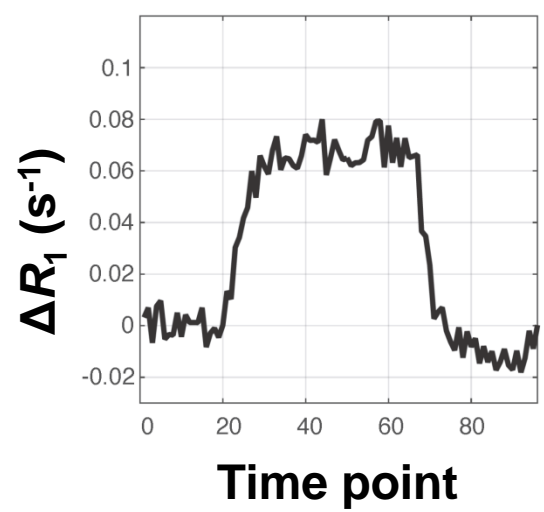
**Sub-regional  $\Delta R_1$**

**Tumor composition**

**A**



**B**



**C**

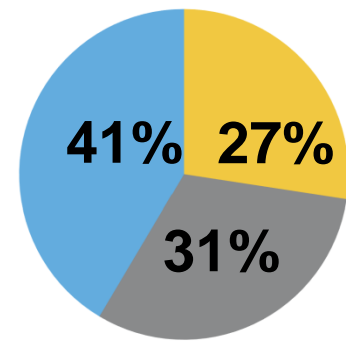
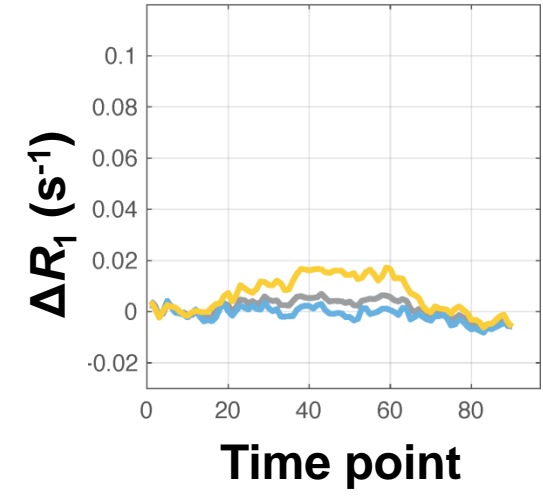
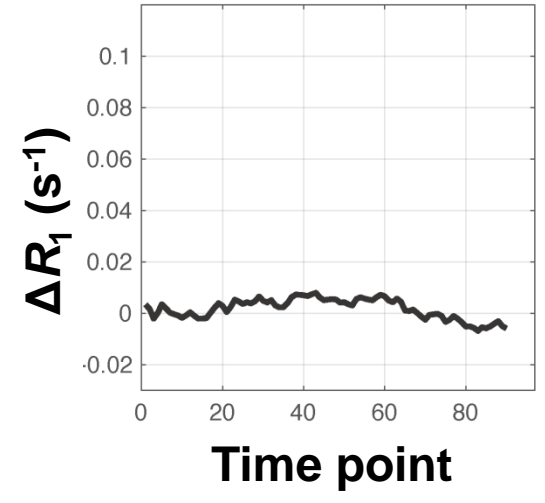
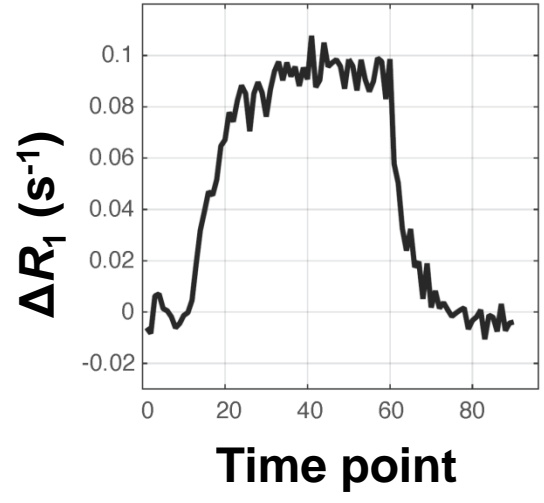
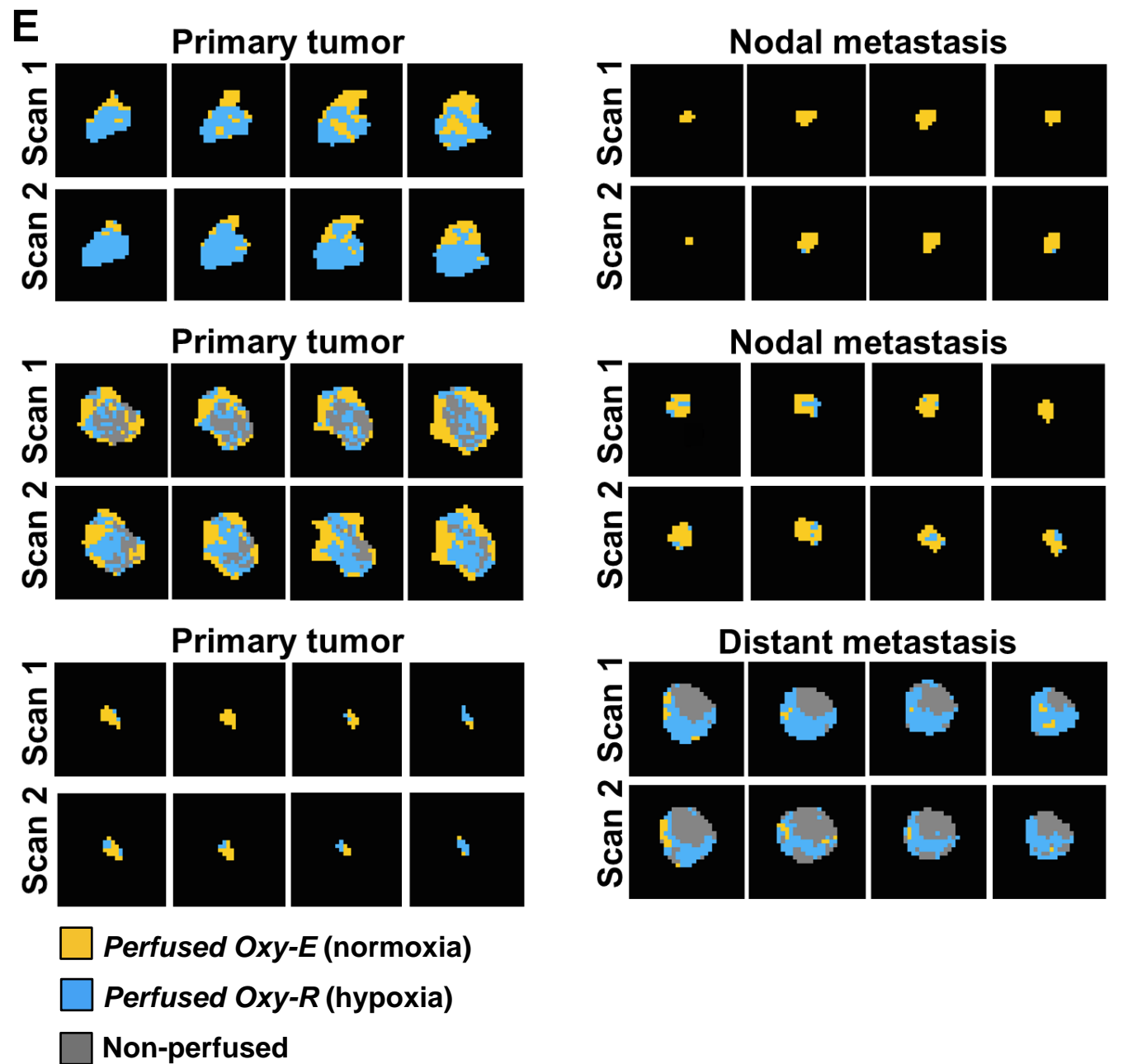
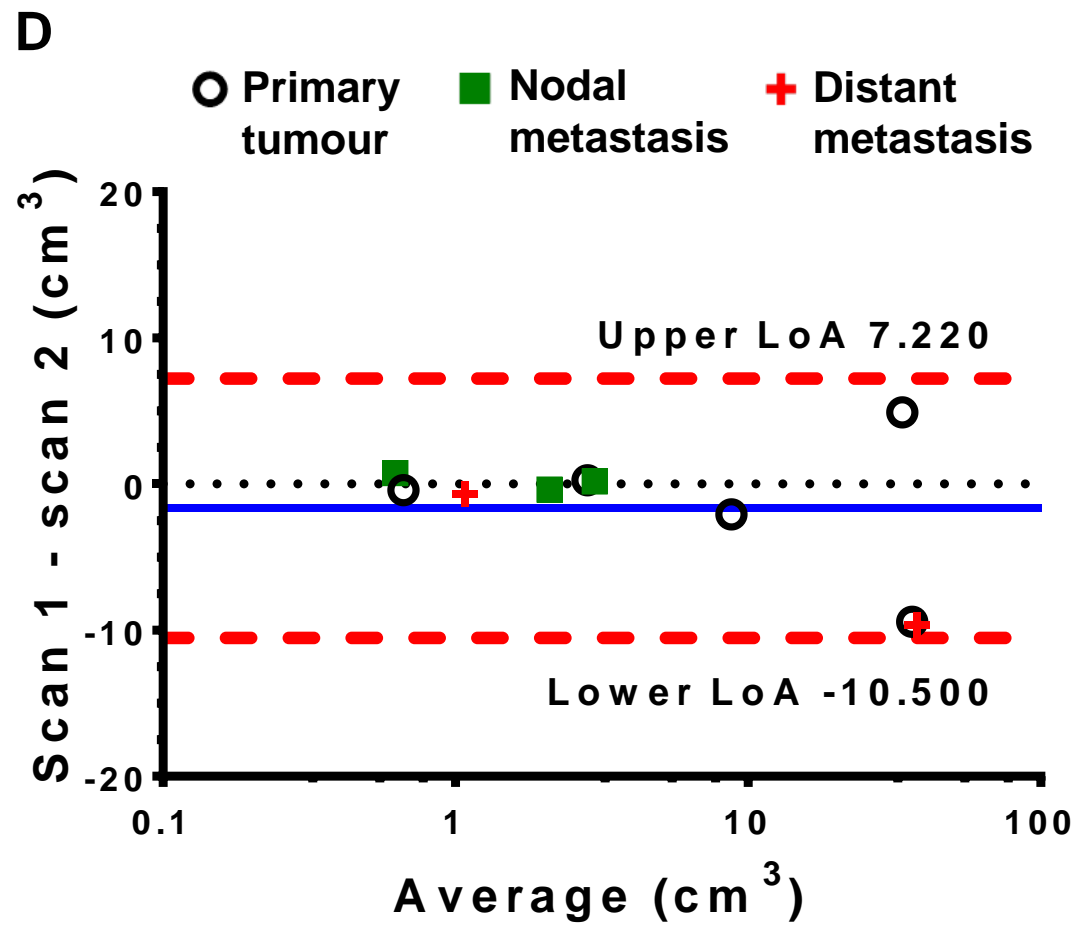


**FIGURE 4**



# A FIGURE 5

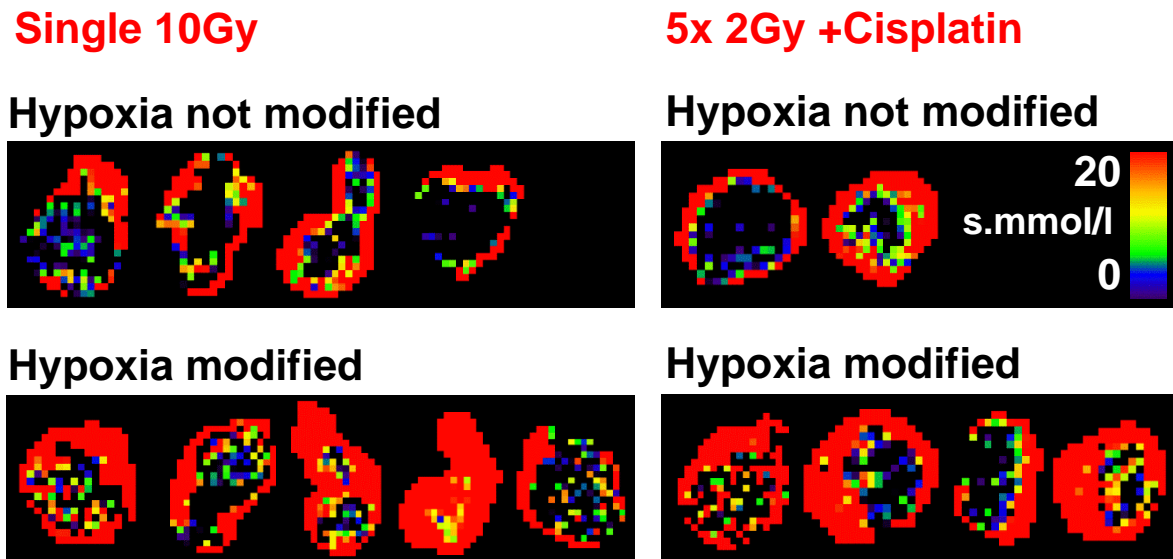
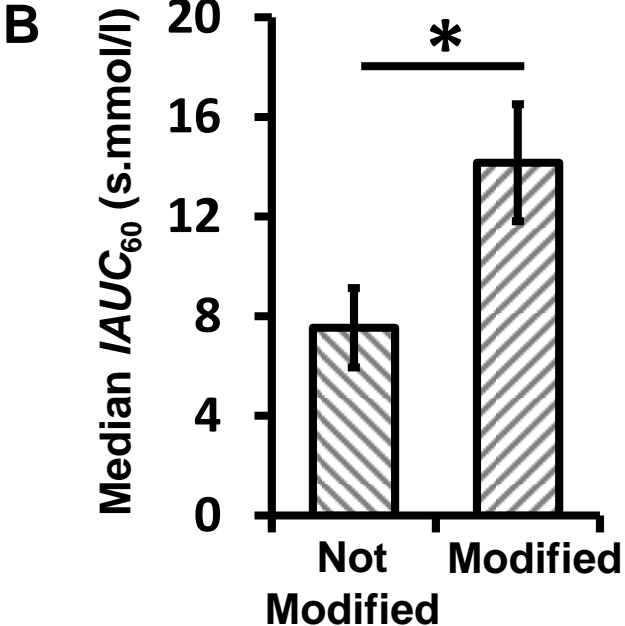
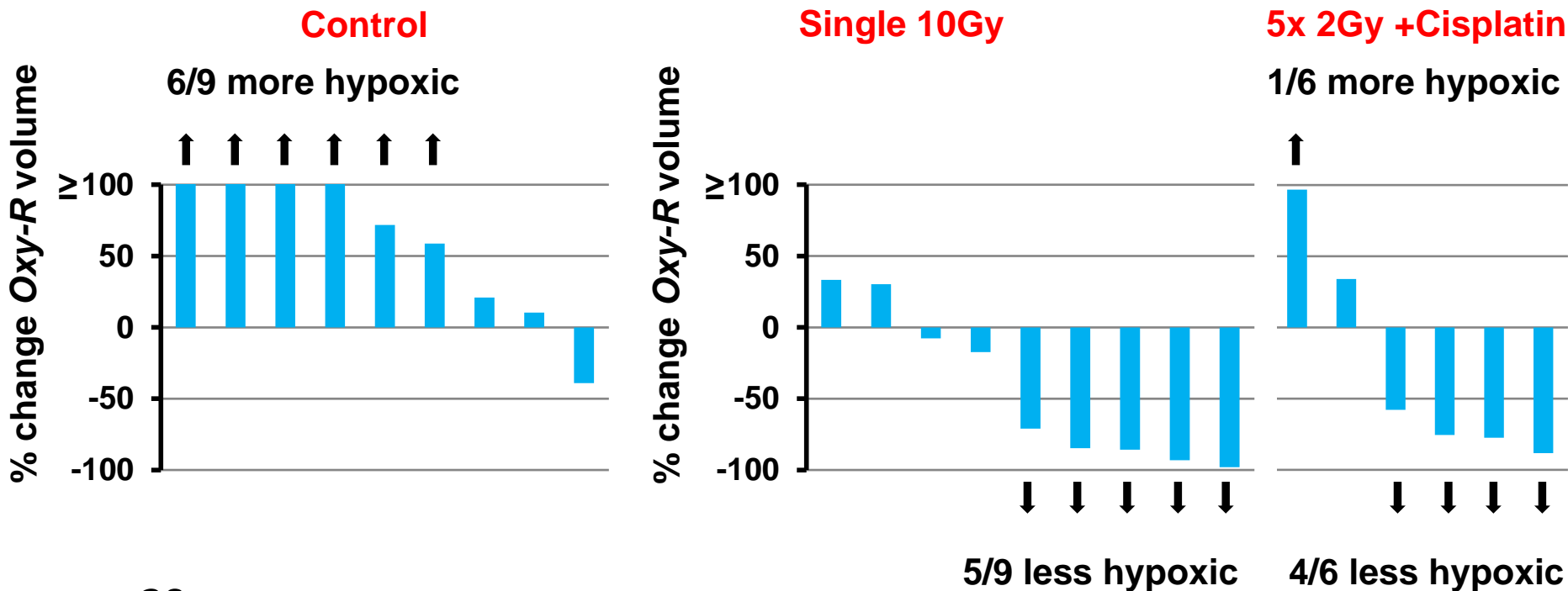
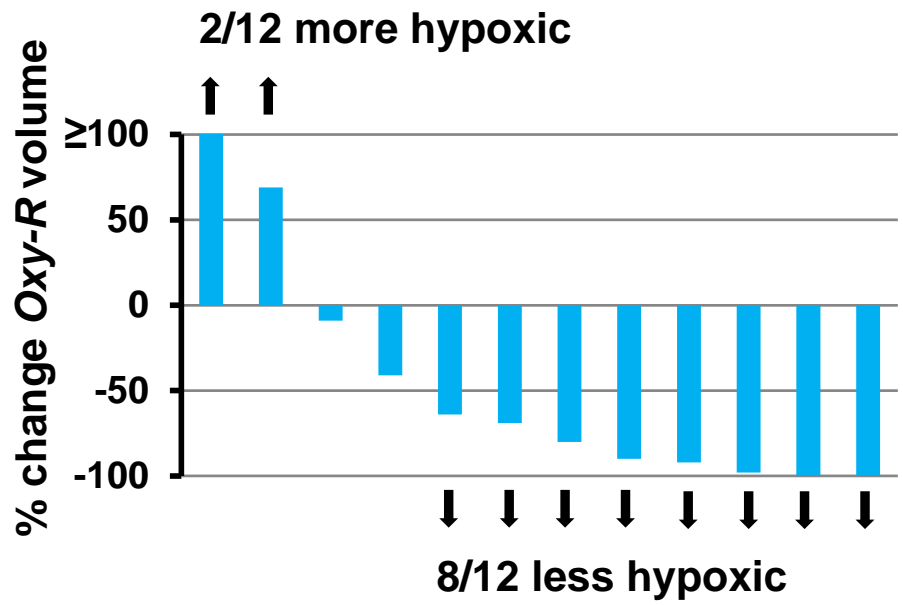


**FIGURE 5**

**C**



**D**

